

# Measurement Report: Enhanced contribution of photooxidation to dicarboxylic acids in urban aerosols during the COVID-19 lockdown in Jinan, East China

Jingjing Meng<sup>1,2</sup>, Yachen Wang<sup>1</sup>, Yuanyuan Li<sup>1</sup>, Tonglin Huang<sup>1</sup>, Zhifei Wang<sup>3</sup>, Yiqiu, Wang<sup>4</sup>, Min Chen<sup>1</sup>, Zhanfang Hou<sup>1</sup>, Kimitaka Kawamura<sup>5</sup>, Pingqing Fu<sup>2</sup>

<sup>1</sup>School of Geography and Environment, Liaocheng University, Liaocheng 252000, China

<sup>2</sup>Institute of Surface-Earth System Science, School of Earth System Science, Tianjin University, Tianjin 300072, China

<sup>3</sup>Jinan Environmental Monitoring Center of Shandong Province, Jinan 250101, China

<sup>4</sup>Liaocheng Environmental Information and Monitoring Center, Liaocheng, 252000, China

<sup>5</sup>Chubu Institute for Advanced Studies, Chubu University, Kasugai 487-8501, Japan

Correspondence to: Pingqing Fu (fupingqing@tju.edu.cn)

**Abstract.** To curb the spread of a novel coronavirus pandemic (COVID-19), a preventive lockdown (LCD) policy was first implemented across China in early 2020, resulting in a substantial drop-off in anthropogenic pollutant emissions and thus the amelioration of air quality. Unexpectedly, several haze events driven by enhanced secondary organic aerosols (SOA) still took place in eastern China during the LCD. To investigate the effect of LCD measures on the formation of SOA, PM<sub>2.5</sub> samples were collected before and during the LCD in Jinan, East China. The samples were analyzed for dicarboxylic acids (diacids) and related compounds, water-soluble inorganic ions, carbonaceous species, as well as the stable carbon isotopic compositions ( $\delta^{13}\text{C}$ ) of major diacids. Our results show that despite the sharp decrease of primary pollutants (e.g., CO, SO<sub>2</sub>, NO<sub>2</sub>, and elemental carbon) during the LCD, the O<sub>3</sub> concentration, proportion of secondary inorganic aerosols, concentration levels, and relative abundance of diacid homologues in water-soluble organic compounds (WSOC) were still 2–4 times higher than those before the LCD. The ratios of oxalic acid (C<sub>2</sub>) to diacids (C<sub>2</sub>/diacids) and to total detected organic components were higher during the LCD than those before the LCD, suggesting the more aged organic aerosols during the LCD under the clearer sky conditions. The temporal changes, diurnal variations in major diacids, and their higher concentrations and contributions during the LCD than before the LCD are mainly due to the enhanced photochemical oxidation by the higher O<sub>3</sub> and the stronger solar radiation during the LCD. Interestingly, compound-specific stable carbon isotope ratios ( $\delta^{13}\text{C}$ ) of C<sub>2</sub> and other major diacids show higher values in the nighttime than the daytime before the LCD, which indicates a significant contribution of organic acids via aqueous phase oxidation at night. Source apportionments using the molecular characteristics of organic compounds and positive matrix factorization (PMF) model suggest that the aqueous oxidation (45.2%) and coal combustion (16.7%) were the major sources before the LCD but the photochemical oxidation promoted by the higher O<sub>3</sub> concentration (48.8%) and aqueous oxidation (17.7%) were the dominant source during the LCD. The increased  $\delta^{13}\text{C}$  values of oxalic acid and other major organic acids along with the high ratios of C<sub>2</sub>/Gly, C<sub>2</sub>/mGly, and C<sub>2</sub>/diacids before and during the LCD confirm an isotopic fractionation effect during the precursor oxidation processes. Furthermore, more positive  $\delta^{13}\text{C}$  values of diacids are observed in the daytime than the nighttime during the LCD, which suggests an enhanced photochemical oxidation in the urban atmosphere during this period.

# 1 Introduction

Water-soluble organic compounds (WSOC), constituting a great proportion of atmospheric fine particles, have attracted a growing attention for the adverse effects on haze formation and global climate change (Lv et al., 2022; Wang et al., 2016). Dicarboxylic acids (diacids) and their organic precursors such as oxocarboxylic acids (oxoacids) and  $\alpha$ -dicarbonyls are ubiquitous in the atmosphere, accounting for 14% of WSOC in particulate matter of urban regions (Ho et al., 2007; Kawamura and Bikkina, 2016), and can be up to 52% in the marine area (Bikkina et al., 2015). Due to the high solubility and hygroscopic property, diacid homologues can not only modify the hygroscopic growth of aerosols, but also improve the cloud condensation nuclei (CCN) activation, thus they exert an important effect on radiative forcing of aerosols via scattering the solar radiation and cloud formation (Ding et al., 2021; Wang et al., 2015).

Diacids and related compounds can be emitted directly from biogenic sources (Rinaldi et al., 2011), vehicle exhausts (Kawamura and Kaplan, 1987), and combustions of biomass and fossil fuels (Cao et al., 2017; Narukawa et al., 1999), while their relative contribution to total aerosol mass is negligible (Shen et al., 2022; Wang et al., 2020a). A growing body of evidence from model studies, chamber experiments, cloud observations, and field measurements have highlighted that most of these water-soluble organic acids are predominantly generated from the photochemical oxidation of volatile organic compounds (VOCs) followed by partitioning into the aqueous phase in wet aerosols, fog, and cloud droplets (Carlton et al., 2007; Ervens et al., 2004, 2011; Fu et al., 2008; Lim et al., 2013; Shen et al., 2022; Wang et al., 2010). Therefore, diacid homologues have been regarded as essential indicators of SOA in the atmosphere to trace the aging processes and assess the oxidative capacity of atmosphere (Enami et al., 2015; Zhao et al., 2020). As the lowest molecular weight and the most abundant diacid, oxalic acid ( $C_2$ ) has been proved to be mostly derived from two pathways: (1) photochemical breakdown (or decomposition) of longer-chain diacids ( $C_3$ – $C_{11}$ ) (Enami et al., 2015; Yu et al., 2021); and (2) secondary oxidation of VOCs via  $\alpha$ -dicarbonyls including glyoxal (Gly) and methylglyoxal (mGly) in aqueous phase of aerosol and cloud droplets, which has been considered to dominate over the first pathway (Carlton et al., 2007; Xu et al., 2022).

More oxidized SOA are largely produced from aqueous oxidation, while less oxidized SOA are largely derived from gaseous photochemical oxidation (Hu et al., 2017; Yu et al., 2019). Modeling studies and laboratory experiments also demonstrate the in-cloud  $C_2$  formation (Crahan et al., 2004; Lim et al., 2005; Warneck, 2003) from the oxidation of Gly (Carlton et al., 2007) and other gaseous “Gly-like” precursors such as glycolaldehyde (Perri et al., 2009) and mGly (Altieri et al., 2008) with  $OH \cdot$  radical. Yu et al. (2019) reported that aqueous oxidation exerts a dominant effect on diacids and related compounds despite the increased contribution of photochemical oxidation in gas phase during the haze events in Beijing using multiple linear regression. A recent study by Xu et al. (2022) pointed out that a large portion of  $C_2$  was derived from the aqueous process of organic precursors emitted from fossil fuel combustion. Laboratory simulation has demonstrated that  $C_2$  can be photodegraded under the  $O_3$  chemical pathway (Gligorovski et al., 2010), but field measurements have demonstrated that formation pathways influenced by  $O_3$  are involved in the formation of  $C_2$  (Meng et al., 2021; Mochizuki et al., 2017). The formation mechanism and influencing factors as well as the contribution of aqueous oxidation and gaseous photochemical oxidation are still not well understood. Therefore, further investigations on  $C_2$  and related compounds are necessary to provide a knowledge base for better understanding SOA and improving the accuracy of model.

To curb the transmission of the novel coronavirus disease 2019 (COVID-19) in human society, a strict lockdown (LCD) measure was first implemented by the Chinese government starting at the end of January 2020 (Le et al., 2020). These dramatic restrictions resulted in a sharp drop-off of air pollutants (Li et al., 2021; Meng et al., 2021), for instance, the average concentrations of five parameters including CO,  $NO_2$ ,  $SO_2$ ,  $PM_{2.5}$ , and  $PM_{10}$  decreased by 4.6–24.7% in 44 cities of China because of the travel restrictions during the LCD (Bao and Zhang, 2020). Unexpectedly, a few haze episodes still occurred in China during the LCD. Online observations, model simulations, and satellite measurements have pointed out that the appearance of haze events during the LCD were mainly caused by the unfavorable meteorological conditions, continuous emissions of  $SO_2$ ,  $NO_x$ , and VOCs from power plants and petrochemical refineries, and an enhanced SOA formation (Huang

et al., 2020; Li et al., 2020; Wang et al., 2020b; Shi et al., 2021; Zhong et al., 2021). These studies focused on the effect of  
80 the LCD policies on air quality and haze formation, for example, Le et al. (2020) and Huang et al. (2020) pointed out that the  
reduction of NO<sub>x</sub> emissions lead to the enhanced ozone concentration, further improved the atmospheric oxidizing capacity  
and promoted the formation of secondary aerosol during the LCD. However, little is known about the impact of LCD  
measures on the molecular distributions, aging processes, and the formation mechanisms of SOA from field observations.  
In order to understand the effect of the reduced anthropogenic emissions during the LCD and different meteorological  
85 parameters on the evolutionary process of homologous diacids and to investigate the relative contribution of aqueous  
oxidation versus gas-phase photochemical oxidation to total diacid homologues, we collected fine aerosol samples in urban  
Jinan, East China on a day/night basis before and during the LCD. We compare the differences in the molecular distributions,  
stable carbon isotopic compositions, and formation processes of C<sub>2</sub> and the related SOA before and during the LCD. Then,  
we investigate the effect of meteorological parameters (e.g., RH, temperature, and solar radiation) and aerosol aqueous  
90 properties (e.g., liquid water content (LWC) of aerosol and particle acidity (pH<sub>is</sub>)) on their formation processes in the urban  
atmosphere.

## 2 Experimental methods

### 2.1 Aerosol sampling

Fine aerosol (PM<sub>2.5</sub>) sampling was conducted on the rooftop of a six-story building (36.67° N, 117.06° E, approximately 20 m  
95 above ground) that was about 40 m away from the Jinan Environment Monitoring Center (one of the State Controlling Air  
Sampling Sites in Jinan). The sampling site is in the center of Jinan city, which is located in the midwestern part of  
Shandong Province, China (Fig. S1). The sampling site lies in a typical urban setting surrounded by heavy traffic roads,  
residential areas, and commercial centers. PM<sub>2.5</sub> samples were collected using prebaked (450 °C, 8 h) quartz fiber filters (8 in.  
× 10 in.) from 6 January to 17 February 2020. The government of Shandong Province first performed the preventive LCD  
100 starting on 24 January 2020; thus the whole sampling period was divided into two periods: (1) before the LCD from 6 to 23  
January, (2) during the LCD from 31 January to 17 February. Each sample lasted for 12 h on a day/night basis using a  
high-volume air sampler (TISCH, USA) at an airflow rate of 1.013 m<sup>3</sup> min<sup>-1</sup>. The daytime samples were collected from 8:00  
to 20:00, while nighttime samples were collected from 20:00 to 8:00 the next day. The field blank is sampled to see whether  
the aerosol samples have been polluted during the operation process, including the placing and collecting processes of the  
105 filter, which takes about a few minutes. The operating procedure of collecting field blank samples for 10 min in this study is  
conventional and scientifically sound and was also confirmed in other studies (Qi et al., 2022; Yi et al., 2021). Therefore,  
field blank samples were also collected by mounting the blank filter onto the sampler for 10 min without turning on the  
sampler before, during, and after the sampling campaign, respectively. A total of 72 PM<sub>2.5</sub> samples (36 for daytime and 36  
for nighttime) and 6 field blank samples were collected in the whole sampling period. After the collection, each filter was  
110 sealed in an aluminum foil bag and stored in a freezer (-20 °C) for about 16 months prior to analysis. The concentrations of  
PM<sub>2.5</sub>, PM<sub>10</sub>, CO, SO<sub>2</sub>, NO<sub>2</sub>, and O<sub>3</sub>, as well as meteorological parameters such as wind direction/speed, RH, temperature,  
and solar radiation were retrieved from the monitoring station in the Jinan Environment Monitoring Center  
(<https://www.aqistudy.cn/>). The detail information of quality assurance/quality control (QA/QC) of online data was  
described in Text S4. The inlet height of the air quality monitoring station was approximately 20 m above the ground level.

### 2.2 Chemical Analysis

#### 2.2.1 Determination of diacids and related compounds as well as levoglucosan

The quantitative method for analyzing diacids, oxoacids, and  $\alpha$ -dicarbonyls in PM<sub>2.5</sub> has been described previously (Fu et al.,

2013; Meng et al., 2020). Briefly, a quarter of the filter was extracted with 5 mL pure Milli-Q water under ultrasonication three times. The water extracts were concentrated to near dryness and then reacted with 14%  $\text{BF}_3/n$ -butanol at 100 °C for 1 hour. During this process, the carboxyl functional group was derivatized to butyl ester, and the aldehyde and keto groups were derivatized to dibutoxy acetal. After derivatization, *n*-hexane was added and washed with pure water three times. Finally, the hexane layer was determined by a gas chromatography-mass spectrometry (GC-MS) and quantitatively analyzed using a GC (Agilent 6980) coupled with an HP-5 column (0.2mm  $\times$  25m, 0.5  $\mu\text{m}$  film thickness) and a flame ionization detector (FID). GC-MS was performed on a Hewlett-Packard model Agilent 7890A GC coupled to a Hewlett-Packard model Agilent 5975C mass selective detector (MSD). GC separation was equipped with a split/splitless injector and a fused silica capillary column (DB-5MS, 30 m  $\times$  0.25 mm i.d., 0.25  $\mu\text{m}$  film thickness). The GC oven temperature was programmed from 50°C for 2 min to 120°C at a rate of 15°C  $\text{min}^{-1}$ , and then to 300°C at a rate of 5°C  $\text{min}^{-1}$  with a final hold at 300°C for 16 min. The mass spectrometer was operated on the electron impact (IE) mode at 70 eV and scanned from 50 to 650 Da. The same analytical method as described above was also applied for field blank filters. As described in previous studies, the recoveries of  $\text{C}_2$  ranged from 70% to 83% and other target compounds were better than 80% (Ding et al., 2021; Kawamura et al., 2013; Kawamura and Yasui, 2005; Meng et al., 2020; Zhao et al., 2020). Recoveries of the target compounds in this study were 80% for  $\text{C}_2$  and higher than 85% for other organic species. Therefore, the percent recoveries mentioned in this study were good enough for such analysis.

Additionally, another portion of each filter sample was extracted with a mixture of dichloromethane and methanol (2:1, *v/v*) under ultrasonication. After being derivatized with 60  $\mu\text{L}$  mixture of *N*, *O*-bis-(trimethylsilyl) trifluoroacetamide (BSTFA) and pyridine (5:1, *v/v*) at 70°C for 3 h, the derivatized extracts were identified for levoglucosan using a GC-MS (Yi et al., 2021). The recovery rate of levoglucosan is higher than 95%. Compared with the ambient samples, the concentration of levoglucosan in the field blank samples was lower than 4%. The data of targeted organic species presented in this study were corrected for both recoveries and field blanks.

### 2.2.2 Stable carbon isotopic composition of diacids and related compounds

The stable carbon isotopic compositions ( $\delta^{13}\text{C}$ ) of major diacids and related compounds were measured using the method reported elsewhere (Kawamura and Watanabe, 2004). Briefly, 2  $\mu\text{L}$  internal standard (*n*- $\text{C}_{13}$  alkane, -27.24 ‰) was spiked to the ester fraction, and the  $\delta^{13}\text{C}$  values of the derivatized samples relative to Pee Dee Belemnite (PDB) were identified using a GC-isotope ratio MS (GC-IR-MS, Thermo Fisher, Delta V Advantage). GC was installed with a HP manual on-column injector and a capillary column (CIP-Sil 8CB, 60 m  $\times$  0.32 mm  $\times$  0.25  $\mu\text{m}$ ) was used with a column oven temperature programmed from 50 to 120°C at a rate of 30°C  $\text{min}^{-1}$  and then to 300°C at a rate of 6°C  $\text{min}^{-1}$ . Flow rate of carrier gas (He) was maintained at 1.7 mL  $\text{min}^{-1}$ . Each sample was measured twice or three times to check the analytical error of the  $\delta^{13}\text{C}$  values, which were less than 0.2‰. The  $\delta^{13}\text{C}$  values were then calculated for free organic acids using an isotope mass balance equation based on the measured  $\delta^{13}\text{C}$  values of derivatives and the derivatizing agent ( $\text{BF}_3/n$ -butanol), as detailed in Text S1 (Kawamura and Watanabe, 2004).

### 2.2.3 Elemental carbon (EC), organic carbon (OC), WSOC, and inorganic ions

EC and OC in the  $\text{PM}_{2.5}$  samples were analyzed using a DRI Model 2015 Carbon Analyzer following the Interagency Monitoring of Protected Visual Environments (IMPROVE) thermal/optical reflectance (TOR) protocol (Chow et al., 2004). As for the measurement of inorganic ions and WSOC, an aliquot of each sample filter was extracted with 30 mL Milli-Q water using an ultrasonic bath three times, and then filtered through PTFE filters to remove particles and filter debris. The water extract was then divided into two parts. One part was analyzed for inorganic ions using an ion chromatography (Dionex 600, USA), and the other part was used to determine WSOC using a Total Carbon Analyzer (TOC-L CPH, Shimadzu, Japan).

## 2.3 Calculation of aerosol liquid water content (LWC) and particle in-situ pH (pH<sub>is</sub>)

160 As for the calculation of aerosol LWC and pH<sub>is</sub>, the ISORROPIA-II model that treated the Na<sup>+</sup> - NH<sub>4</sub><sup>+</sup> - K<sup>+</sup> - Ca<sup>2+</sup> - Mg<sup>2+</sup> - SO<sub>4</sub><sup>2-</sup> - NO<sub>3</sub><sup>-</sup> - Cl<sup>-</sup> system was applied. The forward mode with a metastable state in the ISORROPIA model was adopted (Fountoukis and Nenes, 2007).

## 3 Results and Discussion

### 3.1 Overview of observations

165 Temporal variations in the concentrations of PM<sub>2.5</sub>, PM<sub>10</sub>, gaseous pollutants, major chemical components of PM<sub>2.5</sub>, and meteorological parameters before and during the LCD are summarized in Table 1 and presented in Fig. 1. Both temperature and solar radiation exhibited a continuously increasing trend, whereas RH before the LCD was 1.4 times higher than that during the LCD. Wind speed ( $3.0 \pm 0.7 \text{ m s}^{-1}$ ) before the LCD was smaller than that ( $3.7 \pm 1.1 \text{ m s}^{-1}$ ) during the LCD (Table 1), suggesting that air pollution caused by emissions from the local and surrounding regions of Jinan city before the LCD  
170 was greater than that during the LCD, which was supported by the results of backward trajectory and PSCF analysis (Fig. S1).

The parameters of air quality including PM<sub>2.5</sub>, PM<sub>10</sub>, CO, SO<sub>2</sub>, and NO<sub>2</sub> reduced by 39–62% during the LCD (Table 1, Fig. 1), suggesting that the air quality was better during the LCD because of the substantial reduction of anthropogenic emissions. O<sub>3</sub> in Chinese megacities during the wintertime is primarily produced from the NO<sub>x</sub>-saturated regime because of the lack of HO<sub>x</sub> radical (Li et al., 2021). Being opposite to other five air-quality parameters, O<sub>3</sub> concentration ( $66 \pm 21 \mu\text{g m}^{-3}$ ) during  
175 the LCD increased by 2.3 times compared to that ( $29 \pm 18 \mu\text{g m}^{-3}$ ) before the LCD (Table 1). O<sub>3</sub> is produced from nonlinear processes, and O<sub>3</sub> in Chinese cities is largely produced from NO<sub>x</sub> (NO + NO<sub>2</sub>)-saturated regime attributed to the scared HO<sub>x</sub> radicals during the wintertime (Le et al., 2020). The significant drop of NO<sub>2</sub> during the LCD resulted in the reduction of NO concentration (Xu et al., 2020), and further alleviated the efficient titration effect of O<sub>3</sub> (Levy et al., 2014). Thus, the lower  
180 concentration of NO<sub>2</sub> during the LCD could lead to an increase in O<sub>3</sub> concentration. Besides, O<sub>3</sub> exhibited a negative correlation with PM<sub>2.5</sub> mass concentration ( $R^2 = 0.57$ ) during the LCD, due to the weakened aerosol radiative effect on the photochemical formation of O<sub>3</sub> (Wu et al., 2020) and the reduced precursors of O<sub>3</sub> (Li et al., 2019). The more favorable atmospheric conditions such as the higher temperature and stronger solar radiation during the LCD were beneficial for the generation and accumulation of O<sub>3</sub> (Li et al., 2019). A recent study using the WRF–Chem model found that about 80% of  
185 the increased O<sub>3</sub> level in eastern China was mainly due to meteorological changes, and only 20% resulted from the reduced pollutant emissions (Wang et al., 2022).

The decreased concentrations of EC, OC, and WSOC in PM<sub>2.5</sub> but the enhanced ratios of OC/EC and WSOC/OC during the LCD (Table 1, Fig. 1) indicated more SOA productions due to the stronger photochemical oxidation during the LCD (Zhong et al., 2021). As a key tracer for biomass burning, levoglucosan showed a positive relationship with OC, EC, and WSOC ( $R^2 \geq 0.45$ ) before the LCD rather than during the LCD ( $R^2 \leq 0.15$ ) (Table S1), suggesting that biomass burning played an  
190 important role on carbonaceous species before the LCD rather than during the LCD. Secondary inorganic ions (SIA, total concentration of SO<sub>4</sub><sup>2-</sup>, NO<sub>3</sub><sup>-</sup>, and NH<sub>4</sub><sup>+</sup>) were dominant components of PM<sub>2.5</sub>, which accounted for the higher percentages ( $47 \pm 8\%$ ) in PM<sub>2.5</sub> mass during the LCD than that ( $40 \pm 6\%$ ) before the LCD, indicating an enhanced formation of secondary aerosols during the LCD. The Results of backward trajectory analysis showed that air masses before and during  
195 the LCD in Jinan were different (Fig. S1). Thus, the differences in above chemical species and ratios may be not only because of different emission strengths and types of sources, but also due to different air masses between these two periods. The LWC concentration of aerosol is determined by RH and SIA concentration (Meng et al., 2020). Given the higher RH and SIA concentration before the LCD, the LWC concentration ( $35 \pm 33 \mu\text{g m}^{-3}$ ) before the LCD was 3.4 times higher than

that ( $10 \pm 10 \mu\text{g m}^{-3}$ ) during the LCD. However,  $\text{pH}_{\text{is}}$  remained similar before ( $3.2 \pm 3.0$ ) and during the LCD ( $3.5 \pm 3.5$ ) with no significant statistical difference ( $p > 0.05$ , Table S2), indicating an insignificant difference in atmospheric aerosol acidity before and during the LCD.

### 3.2 Molecular distributions of diacids and related species

A homogeneous series of diacids ( $\text{C}_2\text{--C}_{11}$ ), oxoacids, and  $\alpha$ -dicarbonyls identified in  $\text{PM}_{2.5}$  samples before and during the LCD are summarized in Table 2. To avoid the effect of atmospheric dilution due to the boundary layer height variations, here we use the ratios of SOA species to EC or CO to explore the secondary production of organic species (Yu et al., 2021). As shown in Fig. 2, the ratio of total concentration of detected organic components (TDOCs) normalized by CO (TDOCs/CO) increased exponentially with the increase of temperature before ( $y = 257.46e^{0.019x}$ ,  $R^2 = 0.56$ , Fig. 5a) and during ( $y = 301.49e^{0.067x}$ ,  $R^2 = 0.58$ , Fig. 5c) the LCD, which was consistent with the Arrhenius Law, confirming that TDOCs in this study were primarily derived from secondary formation and the contribution of primary emissions was insignificant. TDOCs are considered as stable products of secondary oxidation for a number of hydrocarbons (Martinelango et al., 2007). The loss of diacids (e.g.,  $\text{C}_2$ ) through the photolysis of iron oxalate complexes is a dominant sink from field observations and model studies (Cheng et al., 2017; Pavuluri and Kawamura, 2012; Weller et al., 2014; Zhou et al., 2015), while these species are stable in the absence of Fe (Kunwar et al., 2019). Previous studies have pointed out that diacids and related compounds presented a strong correlation with temperature, emphasizing the significance of secondary formation of those compounds with the increase of temperature (Kawamura and Bikkina, 2016; Kawamura and Yasui, 2005; Meng et al., 2014, 2018). Therefore, the loss of diacids and related compounds may be negligible when the temperature increases. Additionally, the exponent number (0.067) of the regression trend line during the LCD was 3.5 times higher ( $p < 0.05$ ) than that (0.019) before the LCD, indicating that the oxidation rate during the LCD was larger. Different secondary formation rates of TDOCs between these two observation periods were largely due to different meteorological factors (e.g., temperature, solar radiation, and RH), oxidants (e.g.,  $\text{O}_3$  and  $\text{OH} \cdot$  radical), emission strengths and types of organic precursors, physicochemical properties of aerosols (e.g.,  $\text{pH}_{\text{is}}$  and LWC), and other influencing factors.

To verify if the concentrations of target compounds and major ratios were of significant difference, statistic tests were performed for  $\text{PM}_{2.5}$  samples before and during the LCD (Table S2 and Table S3). As shown in Table S2, the concentrations of organic species (except for  $\alpha$ -dicarbonyls) and major ratios in  $\text{PM}_{2.5}$  before and during the LCD presented  $p$  values less than 0.05, indicating that the abundances and compositions of the major species before and during the LCD were statistically different. TDOCs exhibited an upward trend from  $437 \pm 117 \text{ ng m}^{-3}$  ( $246 - 833 \text{ ng m}^{-3}$ ) before the LCD to  $486 \pm 144 \text{ ng m}^{-3}$  ( $179 - 825 \text{ ng m}^{-3}$ ) during the LCD (Table 2). The concentrations of diacids and oxoacids during the LCD increased by 1.1 and 2.1 times, respectively, while  $\alpha$ -dicarbonyls during the LCD was almost the same as that before the LCD. The concentrations of diacids and TDOCs in this study were significantly lower than those in Xi'an (Cheng et al., 2013), Chengdu (Li et al., 2015), Tianjin (Devineni et al., 2023; Zhao et al., 2023), Liaocheng (Meng et al., 2020), 14 Chinese cities, and other Asian megacities such as Padori, Daejeon (Zhao et al., 2023), Ulaanbaatar (Jung et al., 2010), Chennai (Pavuluri et al., 2010), and Tokyo (Kawamura and Yasui, 2005), but similar to those in Beijing (Zhao et al., 2018) and Guangzhou (Ho et al., 2011) during the wintertime (Table S4).

The daytime concentration of diacids before the LCD was 17% lower than that at night, which was opposite to the diurnal variation of diacids concentration during the LCD (Fig. 3a). As the predominant species throughout the whole observation period,  $\text{C}_2$  concentration increased from  $181 \pm 47 \text{ ng m}^{-3}$  before the LCD to  $239 \pm 108 \text{ ng m}^{-3}$  during the LCD (Table 2), despite of the significant decrease in the primary pollutants from anthropogenic emissions during the LCD.  $\text{C}_2$  is an end product derived from photochemical decomposition of longer-chain diacids or secondary oxidation of  $\alpha$ -dicarbonyls and oxoacids, thus the ratios of  $\text{C}_2$ /diacids and  $\text{C}_2$ /TDOCs can be considered essential tracers for aerosol aging (Wang et al., 2012; Zhao et al., 2020). Both ratios of  $\text{C}_2$ /diacids and  $\text{C}_2$ /TDOCs during the LCD were higher than those before the LCD (Fig. 3b),

reflecting the more aged organic aerosols during the LCD. Therefore, the concentration of  $C_2$  as well as its relative abundance in total diacids and TDOCs were higher during the LCD than those before the LCD, mainly due to the accelerated formation of  $C_2$  during the LCD, which could offset the drop of organic precursors from anthropogenic emissions (Huang et al., 2020). Moreover, the daytime concentration of  $C_2$  and the ratios of  $C_2$ /TDOCs and  $C_2$ /diacids were lower than those at night before the LCD but the opposite trends were found during the LCD, being consistent with the diurnal changes of total diacids before and during the LCD (Fig. 3). The second most abundant diacid was succinic acid ( $C_4$ ), followed by malonic acid ( $C_3$ ) and azelaic acid ( $C_9$ ) before the LCD, while the second dominant diacid during the LCD was  $C_3$ , followed by  $C_4$  and phthalic acid (Ph) (Table 2). Our results suggest that these species had different sources and underwent different formation processes because of different concentration levels of organic precursors and meteorological conditions before and during the LCD. Both ratios of  $C_2/C_4$  and  $C_3/C_4$  have been used as indicators of photochemical aging of diacids, because the hydroxylation of  $C_4$  can be photodegraded into  $C_3$  through the decarboxylation process, and  $C_3$  can be photochemically oxidized into  $C_2$  via intermediates (e.g., ketomalonic ( $kC_3$ ) and hydroxymalonic acids) (Kawamura and Bikkina, 2016; Wang et al., 2010). Both  $C_2/C_4$  ( $8.4 \pm 3.4$ ) and  $C_3/C_4$  ( $1.6 \pm 0.4$ ) ratios during the LCD were higher than those ( $3.9 \pm 1.5$ ,  $0.3 \pm 0.1$ ) before the LCD (Fig. 3b), indicating the stronger photochemical transformation of organic aerosols during the LCD. The  $C_3/C_4$  ratio before the LCD was lower than that in other Asian megacities such as 14 Chinese cities (Ho et al., 2007), Beijing (Zhao et al., 2018), Daejeon (Devineni et al., 2023), and Chennai (Pavuluri et al., 2010), but comparable to that in Tianjin where biomass burning, biogenic sources, and their aging contributed significantly to diacids and related compounds (Devineni et al., 2023) (Table S4). However, the  $C_3/C_4$  ratio during the LCD was much higher than that in other Asian megacities (Table S4), again implying the significantly enhanced photochemical oxidation during the LCD. Previous studies have demonstrated that the  $C_3/C_4$  ratio presented a strong correlation with temperature when the contribution of local sources predominates over long-distance transport (Kawamura and Usukura, 1993; Pavuluri et al., 2010a; Wang et al., 2020). In this study, the  $C_3/C_4$  ratio was correlated strongly with temperature before the LCD ( $R^2 = 0.54$ , Fig. 4a), indicating that diacids before the LCD were largely influenced by local sources. However, the  $C_3/C_4$  ratio was correlated moderately with temperature ( $R^2 = 0.33$ , Fig. 4b) during the LCD, suggesting that the contribution of local sources was equal to that of long-range transport to diacids during the LCD. These results were consistent with the results of backward trajectory and PSCF analysis (Fig. S1). The higher ratios of  $C_2/C_4$  and  $C_3/C_4$  during the LCD may be due to the local photooxidation and aging effects of long-distance transport.

Azelaic acid ( $C_9$ ) is primarily derived from the secondary oxidation of unsaturated fatty acids (e.g., oleic acid) with a double bond at the C-9 position (Kawamura and Usukura, 1993), which is abundant in the fresh and aged aerosols emitted from biomass burning (Shen et al., 2022). It is noteworthy that  $C_9$  concentration ( $12 \pm 4.0$ ) before the LCD was 2.0 times higher than that ( $5.9 \pm 4.8$ ) during the LCD (Table 2), which was consistent with the variation of levoglucosan concentration (Table 1).  $C_9$  showed a more robust relationship with levoglucosan before the LCD ( $R^2 = 0.74$ ) than that ( $R^2 = 0.06$ ) during the LCD (Table S1), suggesting that biomass burning was an essential contributor to  $C_9$  before the LCD rather than during the LCD. Ph is primarily derived from the photochemical degradation of aromatic hydrocarbons (e.g., naphthalene) emitted from anthropogenic sources (Kawamura and Usukura, 1993). Although Ph was the most abundant diacid except for  $C_2$ – $C_4$  during the LCD, its concentration ( $8.8 \pm 6.1 \text{ ng m}^{-3}$ ) and relative abundance ( $2.3 \pm 2.2\%$ ) during the LCD were lower than those ( $11.0 \pm 6.1 \text{ ng m}^{-3}$ ,  $3.2 \pm 1.5\%$ ) before the LCD (Table 2, Fig. 3), suggesting the remarkable drop of anthropogenic emissions during the LCD.

As the important intermediate compounds of mono-carboxylic acids, oxoacids can ultimately generate diacids through heterogeneous oxidation processes (Wang et al., 2012; Yu et al., 2021). The diurnal variations of oxoacids presented similar patterns with diacids in each period (Fig. 3a). Moreover, oxoacids were correlated well with total diacids in each period, respectively ( $R^2 > 0.5$ , Fig. 2), indicating that oxoacids are the important intermediate species of diacids. The molecular distributions of oxoacids were characterized by the predominance of glyoxylic acid ( $\omega C_2$ ) and pyruvic acid (Pyr) in each

285 period. Previous studies have demonstrated that  $C_2$  in urban aerosols is mainly generated from  $\omega C_2$  via aqueous oxidation (Cheng et al., 2015; Zhao et al., 2018). Therefore,  $C_2$  is positively correlated with  $\omega C_2$  before and during the LCD, respectively ( $R^2 > 0.5$ , Fig. 4).

As the two smallest molecular weight  $\alpha$ -dicarbonyls in the aerosols, glyoxal (Gly) and methylglyoxal (mGly) are originated from the photochemical oxidation of volatile organic compounds such as aromatics, isoprene, and monoterpenes in the gaseous phase, which are then partitioned into the aqueous phase of aerosols, and ultimately are oxidized to relatively lower volatility organic acids (e.g.,  $\omega C_2$ , Pyr, and  $C_2$ ) (Carlton et al., 2007; Fu et al., 2008). Although the anthropogenic source emissions of  $\alpha$ -dicarbonyls decreased dramatically during the LCD, the higher temperature and  $O_3$  concentration during the LCD provided a favorable condition for  $\alpha$ -dicarbonyls productions via secondary oxidation, which could offset the drop of primary emissions. Therefore, the concentration ( $24.7 \pm 10.0 \text{ ng m}^{-3}$ ) of  $\alpha$ -dicarbonyls during the LCD was about equal to that ( $25.1 \pm 13.5 \text{ ng m}^{-3}$ ) before the LCD.

### 295 3.3 Aqueous formation of SOA before the LCD

The nighttime concentrations of  $C_2$ , diacids, and TDOCs exhibited higher values than those during the daytime as discussed above. Such diurnal variations may be ascribed to the descended planetary boundary layer (PBL) height at night, which can cause the enhanced concentrations of  $C_2$  and related SOA. However, the increase in the ratios of  $C_2$ /diacids and  $C_2$ /TDOCs at night indicated that the effect of lowered nighttime PBL height was minor, which could be supported by the insignificant diurnal differences of primary pollutant markers such as  $Na^+$ ,  $Ca^{2+}$ , and  $Mg^{2+}$  ( $p > 0.05$ , Table S3) between the daytime and nighttime. Considering the higher RH and LWC concentration at night, the increased concentrations of  $C_2$  and related SOA during the nighttime may be closely linked to the accelerated aqueous production (Cheng et al., 2015; Meng et al., 2020).

The molecular pattern of TDOCs was predominated by  $C_2$  followed by  $C_4$  and  $C_3$  as discussed above, consistent with the molecular distribution in biomass burning smoke (Kawamura et al., 2013; Kundu et al., 2010; Meng et al., 2020; Sorathia et al., 2018). To explore the contribution of biomass burning to TDOCs, levoglucosan, and  $K^+$  were proposed as reliable markers for biomass burning (Hoffmann et al., 2010; Huang et al., 2006).  $K^+$  is abundant in aerosols emitted from biomass burning (Andreae, 1983), thus  $K^+$  exhibited a close correlation with levoglucosan ( $R^2=0.77$ , Table S1) before the LCD. There was no obvious diurnal difference of levoglucosan and  $K^+$  between daytime ( $140 \pm 54.9 \text{ ng m}^{-3}$ ,  $2.0 \pm 0.1 \text{ } \mu\text{g m}^{-3}$ ) and nighttime ( $141 \pm 84.4 \text{ ng m}^{-3}$ ,  $2.1 \pm 0.4 \text{ } \mu\text{g m}^{-3}$ ), suggesting that the higher concentrations of  $C_2$  and related SOA at night were irrelevant to the difference in the emission strength of organic precursors from biomass burning in the daytime and nighttime.  $C_2$ , diacids, and TDOCs exhibited strong correlations with levoglucosan and  $K^+$  before the LCD ( $R^2 > 0.5$ ), while such correlations were not observed during the LCD ( $R^2 < 0.2$ , Table S1), suggesting that biomass burning was an essential contributor to  $C_2$  and related SOA before the LCD rather than during the LCD. The ratio of  $C_2$ /levoglucosan ( $1.7 \pm 0.6$ ) at night before the LCD exhibited a larger value than that ( $1.3 \pm 0.5$ ) in the day, which was mainly ascribed to the accelerated aqueous formation of  $C_2$  at night (see following discussions in Section 3.3). Moreover, the mean values of  $C_2$ /levoglucosan ( $1.5 \pm 0.6$ ),  $C_2/K^+$  ( $0.2 \pm 0.03$ ),  $C_4$ /levoglucosan ( $0.4 \pm 0.1$ ), and  $C_4/K^+$  ( $0.05 \pm 0.02$ ) ratios before the LCD were higher than those (0.05, 0.05, 0.03, 0.03) in fresh particles emitted from savanna fires of southern African (Gao et al., 2003). It is interesting to note that the average ratios of  $C_2/C_4$  ( $3.9 \pm 1.5$ ),  $C_3/C_4$  ( $0.3 \pm 0.1$ ), and  $C_2$ /diacids ( $0.52 \pm 0.55$ ) before the LCD were almost equal to those (3.8, 0.3, and 0.55) measured in the aerosols for two days aging biomass samples via chamber experiment (Shen et al., 2022), suggesting that  $C_2$  and related SOA before the LCD were linked tightly to the secondary oxidation of organic precursors emitted from biomass burning.

To explore the formation pathways and contributing factors of  $C_2$  and related SOA before the LCD, the temporal variations of major diacids, LWC,  $pH_{is}$ , and meteorological parameters (e.g., solar radiation, temperature, and RH) were illustrated in Fig. 5. The  $SO_4^{2-}$  formation was largely from aqueous phase oxidation (see Text S5), thus the correlation analysis between  $SO_4^{2-}$  and  $C_2$  can be used to evaluate the formation process of  $C_2$  mainly via aqueous phase pathways (Sorathia et al., 2018).



$C_2$  was correlated significantly with  $SO_4^{2-}$  in the daytime ( $R^2 = 0.53$ ) and nighttime ( $R^2 = 0.66$ ) (Fig. S2) before the LCD, confirming the dominant aqueous-phase formation pathway of  $C_2$ . It is worth noting that the slope of the regression line of  $C_2/SO_4^{2-}$  ratio (0.005) at night was 1.3 times higher than that (0.004) during the daytime (Fig. S2). Both the higher slope and  $C_2$  concentrations indicate a more efficient formation of  $C_2$  at night, largely because the  $C_2$  production requires multiple steps of aqueous oxidation from VOCs while the formation of  $SO_4^{2-}$  requires fewer steps (Miyazaki et al., 2009). Noticeably, the concentrations of  $C_2$  and diacids, as well as  $C_2$ /diacids ratio culminated on the nighttime of January 23, which was characterized by significantly higher LWC concentration ( $172 \mu\text{g m}^{-3}$ ) and RH (86.9%) (Fig. 5). Gly and mGly are gaseous oxidation products of biogenic and anthropogenic VOCs, and both are highly water-soluble (Carlton et al., 2006). In the presence of liquid water, both species can dissolve in the aqueous phase following Henry's law (Myriokefalitakis et al., 2011). The higher RH and LWC concentration were favorable for the partitioning of Gly and mGly from gaseous phase to aqueous phase and forming  $C_2$ . As shown in Fig. 5, the enhanced concentrations of Gly and mGly in  $PM_{2.5}$  before the LCD were observed when RH and LWC increased. Thus,  $C_2$  and its precursors (including Gly and mGly) were positively correlated with RH and LWC, respectively ( $R^2 > 0.45$ , Fig. 4a). Moreover, the ratios of  $C_2$ /Gly and  $C_2$ /mGly also showed a significant correlation with RH and LWC ( $R^2 > 0.4$ , Fig. 4a). Such strong correlations suggest that the higher LWC concentration and RH could not only promote the formations of  $C_2$  and its precursors, but also facilitate the transformation of  $C_2$  from the organic precursors. Therefore, LWC and RH can be regarded as vitally important factors controlling the aqueous production of  $C_2$ . The nighttime concentrations of LWC and RH were higher than those during the daytime, which led to the higher concentration and percentage contribution of  $C_2$  in the nighttime.

Previous studies have reported that  $C_2$  can also be derived from the chain-breaking of longer-chain diacids in the aqueous phase (Kawamura and Usukura, 1993; Miyazaki et al., 2009). However, there was moderate or no serious correlation between  $C_2$  and longer-chain diacids (e.g.,  $C_3$  and  $C_4$ ), respectively ( $R^2 < 0.3$ , Fig. 4a). Furthermore, longer-chain diacids and the ratios of  $C_2/C_3$  and  $C_2/C_4$  exhibited no significant correlation with LWC or RH ( $R^2 < 0.24$ , Fig. 4a). It can be concluded the effect of chain-breaking of longer homologous diacids on aqueous formation mechanism of  $C_2$  was negligible in this study. Numerous studies have reported that the acidic condition of aerosol is beneficial to the BSOA formation such as 2-methylglyceric acid from BVOCs (e.g., isoprene), and ultimately be transformed into  $C_2$  via Gly, mGly, and  $\omega C_2$  in the aqueous phase by acid-catalyzed oxidation reactions (Surratt et al., 2007). Laboratory experiment has pointed out that the acidic environment of aerosol can accelerate the uptake and production of Gly and mGly via acidic-catalyzed heterogeneous oxidation (Jang et al., 2002; Surratt et al., 2007). As shown in Fig. 4a,  $\text{pH}_{\text{is}}$  exhibited pronounced negative relationships with  $C_2$  and its precursors such as Gly and mGly ( $R^2 \geq 0.45$ ), which was also found in other field studies (Cheng et al., 2017; Meng et al., 2014; Wang et al., 2016; Yu et al., 2021), possibly because of the fact that aerosol acidity could favor the productions of  $C_2$  and its precursors. Therefore, we could conclude that  $C_2$  before the LCD was dominantly derived from the acidic-catalyzed aqueous oxidation with  $\alpha$ -dicarbonyls rather than longer-chain diacids determined by RH and LWC. The reaction rate constant ( $3.6 \times 10^8 \text{ M}^{-1} \text{ s}^{-1}$ ) of  $\omega C_2$  with OH· radical to form  $C_2$  is smaller than that ( $2.9 \times 10^9 \text{ M}^{-1} \text{ s}^{-1}$ ) of its anion, glyoxylate, thus the coarse particles during the dust period, which are alkaline, are favorable for the  $C_2$  formation from  $\omega C_2$  (Wang et al., 2015). Tan et al. (2009) reported that acidity had a minor effect on  $C_2$  formation at cloud- and fog-relevant conditions via online experiments. Those findings necessarily conflicted with each other, largely because the concentration levels of organic precursors, acidity, LWC, and other influencing factors were different from the aerosols in our field observations. Therefore, further field measurements of wet aerosols, laboratory experiments, and model simulations are urgently necessary to elucidate the influencing mechanism of acidity on  $C_2$  formation.

### 3.4 Enhanced photochemical formation of SOA during the LCD

As discussed in Section 3.2, the concentrations of  $C_2$ , diacids, and TDOCs as well as the ratio of  $C_2$ /diacids during the LCD were higher than those before the LCD, despite the anthropogenic source strength dropping dramatically during the LCD.

Given the higher  $O_3$  concentration and stronger solar radiation during the LCD (Table 1), it can be expected that the enhanced concentration and contribution of  $C_2$  were driven by the promoted photochemical oxidation, which was supported by the significantly higher  $C_3/C_4$  ratio ( $1.6 \pm 0.4$ ) during the LCD than that ( $0.3 \pm 0.1$ ) before the LCD. Since  $C_3$  can be generated from photochemical oxidation of  $C_4$  in the atmosphere (Kawamura and Bikkina, 2016), the relatively high  $C_3/C_4$  ratio during the LCD (Fig. 3b) indicates that aerosols during the LCD experienced more substantial photochemical aging. Field measurements and chamber experiments have reported that  $C_2$  can be principally originated from photochemical oxidation of  $\alpha$ -dicarbonyls from VOCs driven by  $O_3$  and  $OH \cdot$  radical (Meng et al., 2021; Mochizuki et al., 2017). Bikkina et al. (2021) reported a laboratory production of oxalic and other LMW diacids together with intermediate oxoacids and  $\alpha$ -dicarbonyls by ozonolysis of isoprene. A few studies have observed that the  $OH \cdot$  radical in the North China Plain (e.g., Shandong Province) was higher during the LCD (e.g., in February 2020) than that before the LCD (Gaubert et al., 2021; Kang et al., 2021; Li et al., 2021). The reduced  $NO_x$  during the LCD could lead to higher  $OH \cdot$  radical, because less  $OH \cdot$  radical could be consumed with  $NO_2$  to produce nitric acid (Gaubert et al., 2021). Besides, the elevated  $O_3$  concentration during the LCD could result in the enhanced  $OH \cdot$  radical, as  $OH \cdot$  radical is mainly from the  $O_3$  photolysis with the water vapor in the atmosphere (Kang et al., 2021). It could be concluded that the  $OH \cdot$  radical during the LCD was higher than before the LCD, being consistent with  $O_3$  concentration. Because  $OH \cdot$  radical was unavailable in this work,  $O_3$  was used here as a marker for the oxidant concentration of photochemical oxidation. In addition, solar radiation could also be used as a reliable proxy for photochemical productions of  $C_2$  and other diacids (Deshmukh et al., 2018). In view of the significant escalation of  $O_3$  concentration and solar radiation during the LCD, it could be concluded that the productions of  $C_2$  and related compounds may be closely involved in the photochemical pathways driven by the higher  $O_3$  concentration and stronger solar radiation.

To investigate the formation mechanism and potential sources of  $C_2$  and related SOA during the LCD, the temporal variations in  $C_2$  and its precursors,  $O_3$ , as well as meteorological factors are presented in Fig. 5. It is interesting to note that the highest  $O_3$  concentration was observed on the daytime of January 31 when the concentrations of  $C_2$  and diacids reached their peaks. Moreover, both  $C_2$  and diacids concentrations as well as the  $C_2$ /diacids ratio exhibited robust correlations with  $O_3$  ( $R^2 > 0.5$ , Fig. 4b), respectively, suggesting that  $O_3$  played an important role in the formation of  $C_2$  and other diacids. Additionally,  $C_2$  and diacids concentrations exhibited similar patterns of variations (Fig. 5) and strong correlations ( $R^2 > 0.5$ , Fig. 4b) with solar radiation during the daytime. However, such similarities and strong correlations of those were not observed with temperature ( $R^2 < 0.2$ , Fig. 4b and Fig. 5), suggesting that the effect of temperature on the photochemical formation of  $C_2$  was negligible. The enhancement of temperature can promote the productions of  $C_2$  and its precursors (Meng et al., 2018), while the increase in the temperature can accelerate the volatilization of  $C_2$ , leading to the drop of  $C_2$  concentration in the aerosol phase (Bilde et al., 2015). These results confirmed that  $C_2$  and other diacids were overwhelmingly derived from the photochemical processes driven by the stronger solar radiation,  $O_3$ , and other oxidants such as  $OH \cdot$  radical.

Numerous studies have demonstrated that the longer-chain diacids can be photochemically degraded into  $C_2$  (Kawamura and Bikkina, 2016; Zhao et al., 2020). It is worth noting that  $C_2$  was correlated strongly with longer-chain diacids such as  $C_3$  and  $C_4$ , respectively ( $R^2 > 0.5$ , Fig. 4b). The ratio of  $C_2$ /diacids was correlated strongly with the ratios of  $C_3/C_4$  ( $R^2 = 0.68$ ) and  $C_2/C_4$  ( $R^2 = 0.58$ , Fig. 4b), indicating that  $C_2$  may be largely derived from the photochemical degradation of higher molecular weight homologues of diacids. However, the correlation of the  $C_2$ /diacids ratio with  $(C_3-C_{11})-C/WSOC$  ( $R^2 = 0.12$ ) was weak, primarily because the supply rates of longer-chain diacids have been demonstrated to be faster than their degradation rates of forming  $C_2$  (Zhao et al., 2020).  $C_2$ /diacids ratio was correlated robustly with solar radiation during the daytime ( $R^2 = 0.76$ , Fig. 4b). Previous study suggested that the correlation analysis of  $C_2$ /diacids,  $C_2/C_4$ , and  $C_3/C_4$  with  $O_3$  could indicate the photochemical chain-breaking of longer-chain diacids producing  $C_2$  (Liu et al., 2021). These ratios were observed to be correlated significantly with  $O_3$  ( $R^2 > 0.45$ , Fig. 4b). These results confirm that  $C_2$  during the LCD was

primarily originated from the photochemical degradation of longer-chain homologous diacids that was driven by stronger solar radiation and higher O<sub>3</sub> concentration and other oxidants rather than higher temperature.

The photochemical oxidation of Gly and mGly has been proposed as a considerable regional and global source of C<sub>2</sub> (Carlton et al., 2007; Fu et al., 2008). Gly can be firstly oxidized to ωC<sub>2</sub> and subsequently to C<sub>2</sub>, while mGly can be oxidized to C<sub>2</sub> via Pyr (Wang et al., 2012; Warneck, 2003). The correlations of C<sub>2</sub> with Gly (R<sup>2</sup> = 0.51) and ωC<sub>2</sub> (R<sup>2</sup> = 0.53) were stronger than those with mGly (R<sup>2</sup> = 0.38) and Pyr (R<sup>2</sup> = 0.04) (Fig. 4b). Moreover, the C<sub>2</sub>/Gly ratio was correlated significantly with O<sub>3</sub> (R<sup>2</sup> = 0.49, Fig. 4b), whereas C<sub>2</sub>/mGly ratio exhibited no correlation with O<sub>3</sub> (R<sup>2</sup> = 0.03, Fig. 4b). These results suggest that the photochemical oxidation of Gly via ωC<sub>2</sub> contributed more to the formation of C<sub>2</sub> than the oxidation of mGly via Pyr, in which O<sub>3</sub> and other oxidants may be important influencing factors.

### 3.5 Stable carbon isotopic compositions of diacids

δ<sup>13</sup>C of specific organic acids can provide insights into the photochemical aging (or processing) of organic aerosols due to isotopic fractionation of carbon during the phase partitioning and/or photochemical oxidation (Wang et al., 2020a; Zhang et al., 2016). On average, most of the detected diacid homologues exhibited higher δ<sup>13</sup>C values during the LCD than those before the LCD (Table 3, Fig. 6). A previous study demonstrated that the enhanced δ<sup>13</sup>C values in diacid homologues were found with UV irradiation time (Pavuluri and Kawamura, 2016). Additionally, Shen et al. (2022) reported that the δ<sup>13</sup>C value for C<sub>2</sub> in the 7-d aged biomass samples was higher than in the 2-d aged biomass samples using the combustion chamber. Thus, the enrichment of δ<sup>13</sup>C values in diacid homologues during the LCD was mainly due to the promoted photochemical oxidation driven by the higher O<sub>3</sub> and the stronger solar radiation during the LCD. Similar to the diurnal variations in major diacids' concentrations, the nighttime δ<sup>13</sup>C values of these detected diacids were more positive (or more negative) than those in the daytime before (or during) the LCD, which was ascribed to their different sources and formation processes in these two observation periods. In brief, the δ<sup>13</sup>C values exhibited a decreasing trend as the carbon numbers of diacids increased (Fig. 6), consistent with other observation campaigns elsewhere (Meng et al., 2020; Pavuluri and Kawamura, 2016; Wang and Kawamura, 2006). The mean δ<sup>13</sup>C value (-20 ± 2.5‰) of C<sub>2</sub> was the heaviest in each period (Table 3), which was comparable to that (-20 ± 3.5‰) observed in its surrounding city such as Liaocheng (Meng et al., 2020), and higher than the values obtained in other China's megacities such as Beijing (-23 ± 3.4‰) (Zhao et al., 2018) and Xi'an (PM<sub>2.1</sub>: from -21 to -24‰) (Wang et al., 2012), but smaller than the values measured in the Korea Climate Observatory at Gosan (-16 ± 4.3‰) of East Asia (Zhang et al., 2016) and western Pacific and Southern Ocean (-17 ± 0.8‰) (Wang and Kawamura, 2006) in the winter (Fig. 7). It is worth noting that the average δ<sup>13</sup>C value of C<sub>2</sub> (-22 ± 1.9‰) before the LCD was equal to that (-22 ± 1.2‰) determined in the 2 d biomass samples (Shen et al., 2022) (Fig. 7), confirming that biomass burning and subsequent oxidation exerted an important effect on C<sub>2</sub> before the LCD.

As mentioned above, C<sub>2</sub> can be not only originated from the photochemical breakdown (or decomposition) of C<sub>3</sub> and C<sub>4</sub> via kC<sub>3</sub> and hydroxymalonic acids (hC<sub>4</sub>), but also be derived from the photochemical oxidation of aromatic hydrocarbons via ωC<sub>2</sub>. The positive correlations of the <sup>13</sup>C values of C<sub>2</sub> with mass ratios of C<sub>2</sub>/ωC<sub>2</sub> (R<sup>2</sup> ≥ 0.39) and C<sub>2</sub>/kC<sub>3</sub> (R<sup>2</sup> ≥ 0.37) during the LCD were observed, whereas such robust relations only with C<sub>2</sub>/ωC<sub>2</sub> (R<sup>2</sup> ≥ 0.47) rather than C<sub>2</sub>/kC<sub>3</sub> (R<sup>2</sup> ≥ 0.01) before the LCD were observed (Fig. 8). These results imply that the effect of photochemical decomposition of higher diacid homologues on C<sub>2</sub> before the LCD was minor, which was consistent with the discussions in Section 3.3. The isotopic values of diacids followed the order of C<sub>2</sub> > C<sub>3</sub> > C<sub>4</sub> in each period (Fig. 6), primarily because diacids containing more carbon numbers may be more reactive to oxidants such as O<sub>3</sub> and OH radical in the atmosphere (Aggarwal and Kawamura, 2008). On the other hand, the removal of CO<sub>2</sub>/CO in the processes of C<sub>3</sub> and C<sub>4</sub> reacting with atmospheric oxidants can generate more <sup>13</sup>C-enriched C<sub>2</sub> due to the KIEs (Wang and Kawamura, 2006). The isotopic values of C<sub>9</sub> ranged from -25 to -30‰ before the LCD, whose difference was less distinguished than those of C<sub>2</sub>-C<sub>4</sub> (Table 3). It is worth noting that the δ<sup>13</sup>C values of organic species from marine plankton (-20‰) are higher than those from terrestrial higher plants (C<sub>3</sub> plants:

–27‰). The  $\delta^{13}\text{C}$  values of  $\text{C}_9$  and the strong correlation of  $\text{C}_9$  with levoglucosan before the LCD as discussed above indicate that biomass burning emitting unsaturated fatty acids and subsequent aqueous oxidation was an important contributor to  $\text{C}_9$  in Jinan during the wintertime. The most negative  $\delta^{13}\text{C}$  value among the identified organic species was tPh throughout the entire period, whose  $\delta^{13}\text{C}$  value ( $-35 \pm 3.1\%$ ) was approximately equal to that ( $-35 \pm 5.3\%$ ) in Liaocheng (Meng et al., 2020) and lighter than that ( $-34 \pm 3.4\%$ ) in Beijing (Zhao et al., 2018) of China where the primary emissions from the combustion of plastic wastes is an essential source of tPh. Moreover, the  $\delta^{13}\text{C}$  value of tPh was negatively (one outlier that possessed a relatively high relative abundance of tPh in diacids was removed) in the daytime or poorly correlated with the ratio of tPh/diacids at night before the LCD (Fig. 8f). The  $\delta^{13}\text{C}$  value of tPh presented a negative correlation with the tPh/diacids during the LCD (Fig. 8l). These results suggest that the primary sources of plastic wastes burning exerted a significant impact on tPh in the atmosphere of Jinan.

Similarly, the  $\delta^{13}\text{C}$  value of oxoacids increases as carbon number decreases (Table 3, Fig. 6).  $\omega\text{C}_2$  has the highest  $\delta^{13}\text{C}$  value, followed by Pyr, and  $\omega\text{C}_3$  before and during the LCD. The more pronounced enhancement of  $\delta^{13}\text{C}$  values in  $\text{C}_2$  and  $\omega\text{C}_2$  in each period suggests that  $\text{C}_2$  in Jinan aerosols was mainly originated from aqueous oxidation of  $\omega\text{C}_2$  (Meng et al., 2020). However, the lighter isotope ( $^{12}\text{C}$ ) was more enriched in  $\omega\text{C}_2$  than both Gly and mGly (Table 3) in each period.  $\omega\text{C}_2$  is largely derived from the photochemical oxidation of organic precursors such as  $\alpha$ -dicarbonyls and acetic acid (Carlton et al., 2007).  $^{12}\text{C}$  can be preferentially accumulated in the products in the non-reversible chemical processes (Wang et al., 2012), resulting in the lighter  $\delta^{13}\text{C}$  values of  $\omega\text{C}_2$  than its precursors. mGly was less enriched in  $^{13}\text{C}$  than Gly (Table 3, Fig. 6) in each period, which was attributed to the lower vapor pressure and higher carbon numbers of mGly that may lead to the weaker isotopic fractionation (Zhang et al., 2016).

It is well established that the  $^{13}\text{C}$  values of diacids and related compounds become isotopically heavier in the aging process of organic aerosols (Pavuluri and Kawamura, 2016; Zhang et al., 2016). As mentioned above, the ratios of  $\text{C}_2/\text{Gly}$ ,  $\text{C}_2/\text{mGly}$ , and  $\text{C}_2/\text{diacids}$  are usually considered significant proxies to evaluate the aging of organic aerosols. These ratios exhibited strong correlations with the  $^{13}\text{C}$  values of  $\text{C}_2$  in each period ( $R^2 > 0.4$ , Fig. 8), indicating the production of more  $^{13}\text{C}$ -enriched  $\text{C}_2$  during the aging processes. The less depletion of  $^{13}\text{C}$  in  $\text{C}_2$  of aged organic aerosols conformed to the actual secondary KIE on activated H-atom abstraction by OH radical rather than to the mass dependence of collision frequencies in the gas phase (Enami et al., 2015). Organic species can react with OH radical and other atmospheric oxidants in the atmospheric oxidation reactions, which result in the removal of  $\text{CO}_2/\text{CO}$  containing  $^{12}\text{C}$  and cause the oxidation products more enriched with the heavier isotope  $^{13}\text{C}$  (Narukawa et al., 1999). Therefore, the  $^{13}\text{C}$  values of major diacids and the related compounds during the LCD were less negative than those before the LCD, again demonstrating that the photochemical oxidation was promoted during the LCD because of the higher temperature and  $\text{O}_3$  concentration under the more clear sky conditions.

### 3.6 Comparison of the source fingerprinting before and during the LCD

To further investigate the crucial sources of diacids and related compounds, positive matrix factorization (PMF) was adopted. Detailed information about PMF analysis was described in Text S3. The model stability of the five-factor solution and error estimation diagnostics were detailed in Table S5 and Table S6, respectively. The PMF-resolved source profiles for the five factors before and during the LCD were shown in Fig. 9. Before the LCD,  $\text{C}_2$ ,  $\text{C}_3$ ,  $\omega\text{C}_2$ , Pyr, Gly, mGly, LWC, WSOC,  $\text{NO}_3^-$ ,  $\text{SO}_4^{2-}$ , and  $\text{NH}_4^+$  exhibited the relatively higher loadings in the first factor (Fig. 9a).  $\text{SO}_4^{2-}$  is a representative product of secondary oxidation in the aqueous phase, and LWC had been proved to be a significant influencing factor during the aqueous oxidation as discussed above. Therefore, the first factor was considered the sources from aqueous phase oxidation. The second factor was characterized by the stronger loadings of  $\text{C}_3$ ,  $\text{C}_4$ , Ph, and EC. Ph is generated from the photochemical oxidation of polycyclic aromatic hydrocarbons (e.g., naphthalene) that are primarily emitted from the domestic coal combustion in China's megacities (Zhao et al., 2018), thus the second factor was categorized as a coal combustion source.  $\text{O}_3$  had been confirmed to be a reliable proxy for gaseous photochemical oxidation, thus the robust relationships of  $\text{O}_3$ ,

495  $\alpha$ -dicarbonyls, and  $\omega$ C<sub>2</sub> with the third factor indicated the contribution of gaseous photochemical oxidation. The fourth factor was significantly associated with Mg<sup>2+</sup> and Ca<sup>2+</sup>, which represented dust emission. As an important indicator of biomass burning, levoglucosan was strongly correlated with C<sub>9</sub> and EC in the fifth factor. Although diacids and related compounds can be produced from the secondary oxidation of organic precursors from biomass burning (Cao et al., 2017; Kawamura et al., 2013), biomass burning can directly emit those compounds (Fu et al., 2008; Gao et al., 2003; Kundu et al., 2010; Narukawa et al., 1999; Shen et al., 2022). Thus, the fifth factor could be regarded as a primary source of biomass burning. During the LCD, the first factor was dominated by O<sub>3</sub>, major diacids, and  $\alpha$ -dicarbonyls (Fig. 9b), which represented gaseous photochemical oxidation. The second factor was strongly correlated with C<sub>2</sub>, C<sub>4</sub>, LWC, WSOC, NO<sub>3</sub><sup>-</sup>, SO<sub>4</sub><sup>2-</sup>, and NH<sub>4</sub><sup>+</sup>, suggesting a significant contribution of aqueous oxidation. Levoglucosan, C<sub>9</sub>, EC, and OC presented the stronger loadings in the third factor, indicating a primary source of biomass burning. Mg<sup>2+</sup> and Ca<sup>2+</sup> exhibited strong correlations with the fourth factor, suggesting the sources from dust emission. Ph and EC presented strong correlations with the fifth factor, representing a coal combustion source.

The PMF-resolved relative contributions to the detected species before and during the LCD were presented in Fig. 9c and Fig. 9d, respectively. The aqueous oxidation made the greatest contribution (47.2%) to C<sub>2</sub> and related compounds before the LCD, while it accounted for only 16.1% in the total identified sources during the LCD. The gaseous photochemical oxidation contributed the largest percentage (50.5%) to the total identified sources, confirming that such a source exerted a leading role in the formation of homologous diacids during the LCD, which was in agreement with the results as discussed above. The contribution of biomass burning increased from 11.4% before the LCD to 13.6% during the LCD. However, the contribution of coal combustion decreased from 16.2% before the LCD to 7.2% during the LCD, largely because of the decreased usage of coal for the industry during the LCD.

## 515 **4 Summary and conclusions**

To explore the impact of LCD on the SOA, PM<sub>2.5</sub> aerosols from Jinan, a megacity in East China, before and during the LCD were analyzed for OC, EC, WSOC, inorganic ions, diacids, oxoacids, and  $\alpha$ -dicarbonyls. Due to the sharp dropping in human activities, the air pollutants including PM<sub>2.5</sub>, PM<sub>10</sub>, CO, SO<sub>2</sub>, and NO<sub>2</sub> during the LCD reduced by 39.3–62.4% than those before the LCD. However, the O<sub>3</sub> concentration increased by 1.3 times synchronously during the LCD. The concentrations of diacids and oxoacids during the LCD exhibited upward trends, while  $\alpha$ -dicarbonyls during the LCD was almost equal to that before the LCD. C<sub>2</sub> before the LCD was significantly derived from the acid-catalyzed aqueous phase oxidation of organic precursors emitted from biomass burning where RH and LWC played a significant role. However, C<sub>2</sub> during the LCD was dominantly generated from the photochemical degradation of longer-chain homologous diacids driven by stronger solar radiation and higher O<sub>3</sub> concentration rather than higher temperature. The  $\delta^{13}\text{C}$  values of major detected diacids were more positive during the LCD than before the LCD, with the largest value ( $-20 \pm 2.5\%$ ) for C<sub>2</sub> and the smallest ( $-35 \pm 3.1\%$ ) for tPh. The ratios of C<sub>2</sub>/Gly, C<sub>2</sub>/mGly, and C<sub>2</sub>/diacids exhibited strong correlations with <sup>13</sup>C values of C<sub>2</sub>, indicating the more enriched <sup>13</sup>C in C<sub>2</sub> during the aging processes of organic aerosols. The molecular distributions of diacid homologues and PMF results suggest that TDOCs in Jinan were primarily derived from the aqueous mechanisms of organic precursors emitted from coal combustion and biomass burning before the LCD, while these species were principally derived from the photochemical pathways during the LCD.

*Data availability.* The data in this study are available at: <https://doi.org/10.5281/zenodo.7533247> (Meng et al., 2023).

*Author contribution.* PF designed the study. WY, LY, HT, and CM carried out the experiments and performed the data analysis. JM prepared the manuscript with contributions from all co-authors.

535 *Competing interests.* The authors have the following competing interests: One of the coauthors, Prof. Kimitaka Kawamura is one of the editorial members of this journal.

540 *Acknowledgments.* This work was supported by the National Natural Science Foundation of China (Grant No. 42177083), the Natural Science Foundation of Shandong Province (Grant No. ZR2020MD113), the Junior Faculty Support Program for Scientific and Technological Innovations in Shandong Provincial Higher Education Institutions (2021KJ085), and the Open Funds of State Key Laboratory of Loess and Quaternary Geology, Institute of Earth Environment, Chinese Academy of Sciences (Grant No. SKLLOG2020).

## References

- Aggarwal, S. G. and Kawamura, K.: Molecular distributions and stable carbon isotopic compositions of dicarboxylic acids and related compounds in aerosols from Sapporo, Japan: Implications for photochemical aging during long-range atmospheric transport, *J. Geophys. Res. Atmos.*, 113, D14301, [10.1029/2007jd009365](https://doi.org/10.1029/2007jd009365), 2008.
- 545 Altieri, K. E., Seitzinger, S. P., Carlton, A. G., Turpin, B. J., Klein, G. C., and Marshall, A. G.: Oligomers formed through in-cloud methylglyoxal reactions: Chemical composition, properties, and mechanisms investigated by ultra-high resolution FT-ICR mass spectrometry, *Atmospheric Environment*, 42, 1476-1490, <https://doi.org/10.1016/j.atmosenv.2007.11.015>, 2008.
- 550 Andreae, M. O.: Soot Carbon and Excess Fine Potassium: Long-Range Transport of Combustion-Derived Aerosols, *Science*, 220, 1148, 1983.
- Bao, R. and Zhang, A.: Does lockdown reduce air pollution? Evidence from 44 cities in northern China, *Sci. Total Environ.*, 731, 139052, <https://doi.org/10.1016/j.scitotenv.2020.139052>, 2020.
- Bikkina, S., Kawamura, K., and Miyazaki, Y.: Latitudinal distributions of atmospheric dicarboxylic acids, oxocarboxylic acids, and  $\alpha$ -dicarbonyls over the western North Pacific: Sources and formation pathways, *J. Geophys. Res. Atmos.*, 120, 5010-5035, [10.1002/2014jd022235](https://doi.org/10.1002/2014jd022235), 2015.
- 555 Bikkina, S., Kawamura, K., Sakamoto, Y., and Hirokawa, J.: Low molecular weight dicarboxylic acids, oxocarboxylic acids and  $\alpha$ -dicarbonyls as ozonolysis products of isoprene: Implication for the gaseous-phase formation of secondary organic aerosols, *Sci. Total Environ.*, 769, 144472, <https://doi.org/10.1016/j.scitotenv.2020.144472>, 2021.
- 560 Bilde, M., Barsanti, K., Booth, M., Cappa, C. D., Donahue, N. M., Emanuelsson, E. U., McFiggans, G., Krieger, U. K., Marcolli, C., Topping, D., Ziemann, P., Barley, M., Clegg, S., Dennis-Smith, B., Hallquist, M., Hallquist, Å. M., Khlystov, A., Kulmala, M., Mogensen, D., Percival, C. J., Pope, F., Reid, J. P., Ribeiro da Silva, M. A. V., Rosenoern, T., Salo, K., Soonsin, V. P., Yli-Juuti, T., Prisle, N. L., Pagels, J., Rarey, J., Zardini, A. A., and Riipinen, I.: Saturation Vapor Pressures and Transition Enthalpies of Low-Volatility Organic Molecules of Atmospheric Relevance: From Dicarboxylic Acids to Complex Mixtures, *Chem. Rev.*, 115, 4115-4156, [10.1021/cr5005502](https://doi.org/10.1021/cr5005502), 2015.
- 565 Cao, F., Zhang, S.-C., Kawamura, K., Liu, X., Yang, C., Xu, Z., Fan, M., Zhang, W., Bao, M., Chang, Y., Song, W., Liu, S., Lee, X., Li, J., Zhang, G., and Zhang, Y.-L.: Chemical characteristics of dicarboxylic acids and related organic compounds in PM<sub>2.5</sub> during biomass-burning and non-biomass-burning seasons at a rural site of Northeast China, *Environ. Pollut.*, 231, 654-662, <https://doi.org/10.1016/j.envpol.2017.08.045>, 2017.
- 570 Carlton, A. G., Turpin, B. J., Lim, H.-J., Altieri, K. E., and Seitzinger, S.: Link between isoprene and secondary organic aerosol (SOA): Pyruvic acid oxidation yields low volatility organic acids in clouds, *Geophys. Res. Lett.*, 33,

L06822, 10.1029/2005gl025374, 2006.

- 575 Carlton, A. G., Turpin, B. J., Altieri, K. E., Seitzinger, S., Reff, A., Lim, H.-J., and Ervens, B.: Atmospheric oxalic acid and SOA production from glyoxal: Results of aqueous photooxidation experiments, *Atmos. Environ.*, 41, 7588-7602, <http://dx.doi.org/10.1016/j.atmosenv.2007.05.035>, 2007.
- Cheng, C., Li, M., Chan, C. K., Tong, H., Chen, C., Chen, D., Wu, D., Li, L., Wu, C., Cheng, P., Gao, W., Huang, Z., Li, X., Zhang, Z., Fu, Z., Bi, Y., and Zhou, Z.: Mixing state of oxalic acid containing particles in the rural area of Pearl River Delta, China: implications for the formation mechanism of oxalic acid, *Atmos. Chem. Phys.*, 17, 9519-9533, 10.5194/acp-17-9519-2017, 2017.
- 580 Cheng, C., Wang, G., Meng, J., Wang, Q., Cao, J., Li, J., and Wang, J.: Size-resolved airborne particulate oxalic and related secondary organic aerosol species in the urban atmosphere of Chengdu, China, *Atmos. Res.*, 161-162, 134-142, <http://dx.doi.org/10.1016/j.atmosres.2015.04.010>, 2015.
- Cheng, C., Wang, G., Zhou, B., Meng, J., Li, J., Cao, J., and Xiao, S.: Comparison of dicarboxylic acids and related compounds in aerosol samples collected in Xi'an, China during haze and clean periods, *Atmospheric Environment*, 585 81, 443-449, <http://dx.doi.org/10.1016/j.atmosenv.2013.09.013>, 2013.
- Chow, J. C., Watson, J. G., Chen, L. W. A., Arnott, W. P., Moosmüller, H., and Fung, K.: Equivalence of Elemental Carbon by Thermal/Optical Reflectance and Transmittance with Different Temperature Protocols, *Environ. Sci. Technol.*, 38, 4414-4422, 10.1021/es034936u, 2004.
- 590 Crahan, K. K., Hegg, D., Covert, D. S., and Jonsson, H.: An exploration of aqueous oxalic acid production in the coastal marine atmosphere, *Atmospheric Environment*, 38, 3757-3764, <http://dx.doi.org/10.1016/j.atmosenv.2004.04.009>, 2004.
- Deshmukh, D. K., Mozammel Haque, M., Kawamura, K., and Kim, Y.: Dicarboxylic acids, oxocarboxylic acids and  $\alpha$ -dicarbonyls in fine aerosols over central Alaska: Implications for sources and atmospheric processes, *Atmos. Res.*, 595 202, 128-139, <https://doi.org/10.1016/j.atmosres.2017.11.003>, 2018.
- Devineni, S. R., Pavuluri, C. M., Wang, S., Ren, L., Xu, Z., Li, P., Fu, P., and Liu, C.-Q.: Size-Resolved Characteristics and Sources of Inorganic Ions, Carbonaceous Components and Dicarboxylic Acids, Benzoic Acid, Oxocarboxylic Acids and  $\alpha$ -Dicarbonyls in Wintertime Aerosols from Tianjin, North China, *Aerosol Science and Engineering*, 7, 1-22, 10.1007/s41810-022-00159-0, 2023.
- 600 Ding, Z., Du, W., Wu, C., Cheng, C., Meng, J., Li, D., Ho, K., Zhang, L., and Wang, G.: Summertime atmospheric dicarboxylic acids and related SOA in the background region of Yangtze River Delta, China: Implications for heterogeneous reaction of oxalic acid with sea salts, *Sci. Total Environ.*, 757, 143741, <https://doi.org/10.1016/j.scitotenv.2020.143741>, 2021.
- Enami, S., Hoffmann, M. R., and Colussi, A. J.: Stepwise Oxidation of Aqueous Dicarboxylic Acids by Gas-Phase OH Radicals, *J. Phys., Chem. Lett.*, 6, 527-534, 10.1021/jz502432j, 2015.
- 605 Ervens, B., Feingold, G., Frost, G. J., and Kreidenweis, S. M.: A modeling study of aqueous production of dicarboxylic acids: 1. Chemical pathways and speciated organic mass production, *J. Geophys. Res.*, 109, D15205, 10.1029/2003jd004387, 2004.
- Ervens, B., Turpin, B. J., and Weber, R. J.: Secondary organic aerosol formation in cloud droplets and aqueous particles (aqSOA): a review of laboratory, field and model studies, *Atmos. Chem. Phys.*, 11, 11069-11102, 10.5194/acp-11-11069-2011, 2011.
- 610 Fountoukis, C., and Nenes, A.: ISORROPIA II: a computationally efficient thermodynamic equilibrium model for  $K^+$ - $Ca^{2+}$ - $Mg^{2+}$ - $NH_4^+$ - $Na^+$ - $SO_4^{2-}$ - $NO_3^-$ - $Cl^-$ - $H_2O$  aerosols, *Atmos. Chem. Phys.*, 7, 4639-4659, 10.5194/acp-7-4639-2007, 2007.

- 615 Fu, P., Kawamura, K., Usukura, K., and Miura, K.: Dicarboxylic acids, ketocarboxylic acids and glyoxal in the marine aerosols collected during a round-the-world cruise, *Marine Chemistry*, 148, 22-32, <http://dx.doi.org/10.1016/j.marchem.2012.11.002>, 2013.
- Fu, T.-M., Jacob, D. J., Wittrock, F., Burrows, J. P., Vrekoussis, M., and Henze, D. K.: Global budgets of atmospheric glyoxal and methylglyoxal, and implications for formation of secondary organic aerosols, *J. Geophys. Res.*, 113, D15303, [10.1029/2007jd009505](https://doi.org/10.1029/2007jd009505), 2008.
- 620 Gao, S., Hegg, D. A., Hobbs, P. V., Kirchstetter, T. W., Magi, B. I., and Sadilek, M.: Water-soluble organic components in aerosols associated with savanna fires in southern Africa: Identification, evolution, and distribution, *J. Geophys. Res. Atmos.*, 108, 8491, [10.1029/2002jd002324](https://doi.org/10.1029/2002jd002324), 2003.
- Gaubert, B., Bouarar, I., Doumbia, T., Liu, Y., Stavrakou, T., Deroubaix, A., Darras, S., Elguindi, N., Granier, C., Lacey, F., Müller, J.-F., Shi, X., Tilmes, S., Wang, T., and Brasseur, G. P.: Global Changes in Secondary Atmospheric Pollutants During the 2020 COVID-19 Pandemic, *Journal of Geophysical Research: Atmospheres*, 126, e2020JD034213, <https://doi.org/10.1029/2020JD034213>, 2021.
- 625 Gligorovski, S., Grgić, I., Net, S., Böge, O., Iinuma, Y., Kahnt, A., Scheinhardt, S., Herrmann, H., and Wortham, H.: Light-induced multiphase chemistry of gas phase ozone on aqueous pyruvic and oxalic acids: Aerosol chamber study, *AGU Fall Meeting Abstracts*, 2010.
- 630 Ho, K. F., Cao, J. J., Lee, S. C., Kawamura, K., Zhang, R. J., Chow, J. C., and Watson, J. G.: Dicarboxylic acids, ketocarboxylic acids, and dicarbonyls in the urban atmosphere of China, *J. Geophys. Res. Atmos.*, 112, D22S27, [10.1029/2006jd008011](https://doi.org/10.1029/2006jd008011), 2007.
- Ho, K. F., Ho, S. S. H., Lee, S. C., Kawamura, K., Zou, S. C., Cao, J. J., and Xu, H. M.: Summer and winter variations of dicarboxylic acids, fatty acids and benzoic acid in PM<sub>2.5</sub> in Pearl Delta River Region, China, *Atmos. Chem. Phys.*, 11, 2197-2208, [10.5194/acp-11-2197-2011](https://doi.org/10.5194/acp-11-2197-2011), 2011.
- 635 Hu, W., Hu, M., Hu, W. W., Zheng, J., Chen, C., Wu, Y., and Guo, S.: Seasonal variations in high time-resolved chemical compositions, sources, and evolution of atmospheric submicron aerosols in the megacity Beijing, *Atmos. Chem. Phys.*, 17, 9979-10000, [10.5194/acp-17-9979-2017](https://doi.org/10.5194/acp-17-9979-2017), 2017.
- 640 Huang, X., Ding, A., Gao, J., Zheng, B., Zhou, D., Qi, X., Tang, R., Wang, J., Ren, C., Nie, W., Chi, X., Xu, Z., Chen, L., Li, Y., Che, F., Pang, N., Wang, H., Tong, D., Qin, W., Cheng, W., Liu, W., Fu, Q., Liu, B., Chai, F., Davis, S. J., Zhang, Q., and He, K.: Enhanced secondary pollution offset reduction of primary emissions during COVID-19 lockdown in China, *Natl. Sci. Rev.*, [10.1093/nsr/nwaa137](https://doi.org/10.1093/nsr/nwaa137), 2020.
- Jang, M., Czoschke, N. M., Lee, S., and Kamens, R. M.: Heterogeneous Atmospheric Aerosol Production by Acid-Catalyzed Particle-Phase Reactions, *Science*, 298, 814, 2002.
- 645 Jung, J., Tsatsral, B., Kim, Y. J., and Kawamura, K.: Organic and inorganic aerosol compositions in Ulaanbaatar, Mongolia, during the cold winter of 2007 to 2008: Dicarboxylic acids, ketocarboxylic acids, and  $\alpha$ -dicarbonyls, *Journal of Geophysical Research: Atmospheres*, 115, D22203, [10.1029/2010jd014339](https://doi.org/10.1029/2010jd014339), 2010.
- Kang, M., Zhang, J., Zhang, H., and Ying, Q.: On the Relevancy of Observed Ozone Increase during COVID-19 Lockdown to Summertime Ozone and PM<sub>2.5</sub> Control Policies in China, *Environmental Science & Technology Letters*, 8, 289-294, [10.1021/acs.estlett.1c00036](https://doi.org/10.1021/acs.estlett.1c00036), 2021.
- 650 Kawamura, K. and Bikkina, S.: A review of dicarboxylic acids and related compounds in atmospheric aerosols: Molecular distributions, sources and transformation, *Atmos. Res.*, 170, 140-160, <http://dx.doi.org/10.1016/j.atmosres.2015.11.018>, 2016.
- 655 Kawamura, K. and Kaplan, I. R.: Motor exhaust emissions as a primary source for dicarboxylic acids in Los Angeles ambient air, *Environ. Sci. Technol.*, 21, 105-110, [10.1021/es00155a014](https://doi.org/10.1021/es00155a014), 1987.
- Kawamura, K. and Usukura, K.: Distributions of low molecular weight dicarboxylic acids in the North Pacific aerosol



samples, *J. Oceano.*, 49, 271-283, 10.1007/bf02269565, 1993.

- 660 Kawamura, K. and Watanabe, T.: Determination of Stable Carbon Isotopic Compositions of Low Molecular Weight Dicarboxylic Acids and Ketocarboxylic Acids in Atmospheric Aerosol and Snow Samples, *Anal. Chem.*, 76, 5762-5768, 10.1021/ac049491m, 2004.
- Kawamura, K. and Yasui, O.: Diurnal changes in the distribution of dicarboxylic acids, ketocarboxylic acids and dicarbonyls in the urban Tokyo atmosphere, *Atmospheric Environment*, 39, 1945-1960, <http://dx.doi.org/10.1016/j.atmosenv.2004.12.014>, 2005.
- 665 Kawamura, K., Tachibana, E., Okuzawa, K., Aggarwal, S. G., Kanaya, Y., and Wang, Z. F.: High abundances of water-soluble dicarboxylic acids, ketocarboxylic acids and  $\alpha$ -dicarbonyls in the mountain aerosols over the North China Plain during wheat burning season, *Atmos. Chem. Phys.*, 13, 3695-3734, 10.5194/acpd-13-3695-2013, 2013.
- 670 Kundu, S., Kawamura, K., Andreae, T. W., Hoffer, A., and Andreae, M. O.: Molecular distributions of dicarboxylic acids, ketocarboxylic acids and  $\alpha$ -dicarbonyls in biomass burning aerosols: implications for photochemical production and degradation in smoke layers, *Atmos. Chem. Phys.*, 10, 2209-2225, 10.5194/acp-10-2209-2010, 2010.
- Kunwar, B., Kawamura, K., Fujiwara, S., Fu, P., Miyazaki, Y., and Pokhrel, A.: Dicarboxylic acids, oxocarboxylic acids and  $\alpha$ -dicarbonyls in atmospheric aerosols from Mt. Fuji, Japan: Implication for primary emission versus secondary formation, *Atmospheric Research*, 221, 58-71, <https://doi.org/10.1016/j.atmosres.2019.01.021>, 2019.
- 675 Le, T., Wang, Y., Liu, L., Yang, J., Yung, Y. L., Li, G., and Seinfeld, J. H.: Unexpected air pollution with marked emission reductions during the COVID-19 outbreak in China, *Science*, eabb7431, 10.1126/science.abb7431, 2020.
- Li, L., Li, Q., Huang, L., Wang, Q., Zhu, A., Xu, J., Liu, Z., Li, H., Shi, L., Li, R., Azari, M., Wang, Y., Zhang, X., Liu, Z., Zhu, Y., Zhang, K., Xue, S., Ooi, M. C. G., Zhang, D., and Chan, A.: Air quality changes during the COVID-19 lockdown over the Yangtze River Delta Region: An insight into the impact of human activity pattern changes on air pollution variation, *Sci. Total Environ.*, 732, 139282, <https://doi.org/10.1016/j.scitotenv.2020.139282>, 2020.
- 680 Li, K., Jacob, D. J., Liao, H., Shen, L., Zhang, Q., and Bates, K. H.: Anthropogenic drivers of 2013–2017 trends in summer surface ozone in China, *Proceedings of the National Academy of Sciences*, 116, 422, 10.1073/pnas.1812168116, 2019.
- Li, M., Wang, T., Xie, M., Li, S., Zhuang, B., Fu, Q., Zhao, M., Wu, H., Liu, J., Saikawa, E., and Liao, K.: Drivers for the poor air quality conditions in North China Plain during the COVID-19 outbreak, *Atmospheric Environment*, 246, 118103, <https://doi.org/10.1016/j.atmosenv.2020.118103>, 2021.
- 685 Li, X.-d., Yang, Z., Fu, P., Yu, J., Lang, Y.-c., Liu, D., Ono, K., and Kawamura, K.: High abundances of dicarboxylic acids, oxocarboxylic acids, and  $\alpha$ -dicarbonyls in fine aerosols (PM<sub>2.5</sub>) in Chengdu, China during wintertime haze pollution, *Environmental Science and Pollution Research*, 22, 12902-12918, 10.1007/s11356-015-4548-x, 2015.
- 690 Li, Z., Zhou, R., Wang, Y., Wang, G., Chen, M., Li, Y., Wang, Y., Yi, Y., Hou, Z., Guo, Q., and Meng, J.: Characteristics and sources of amine-containing particles in the urban atmosphere of Liaocheng, a seriously polluted city in North China during the COVID-19 outbreak, *Environ. Pollut.*, 289, 117887, <https://doi.org/10.1016/j.envpol.2021.117887>, 2021.
- 695 Lim, H.-J., Carlton, A. G., and Turpin, B. J.: Isoprene Forms Secondary Organic Aerosol through Cloud Processing: Model Simulations, *Environmental Science & Technology*, 39, 4441-4446, 10.1021/es048039h, 2005.
- Lim, Y. B., Tan, Y., and Turpin, B. J.: Chemical insights, explicit chemistry, and yields of secondary organic aerosol from OH radical oxidation of methylglyoxal and glyoxal in the aqueous phase, *Atmos. Chem. Phys.*, 13, 8651-8667, 10.5194/acp-13-8651-2013, 2013.
- 700 Liu, J., Zhou, S., Zhang, Z., Kawamura, K., Zhao, W., Wang, X., Shao, M., Jiang, F., Liu, J., Sun, X., Hang, J., Zhao, J., Pei, C., Zhang, J., and Fu, P.: Characterization of dicarboxylic acids, oxoacids, and  $\alpha$ -dicarbonyls in PM<sub>2.5</sub> within the

urban boundary layer in southern China: Sources and formation pathways, *Environ. Pollut.*, 285, 117185, <https://doi.org/10.1016/j.envpol.2021.117185>, 2021.

705 Lv, S., Wang, F., Wu, C., Chen, Y., Liu, S., Zhang, S., Li, D., Du, W., Zhang, F., Wang, H., Huang, C., Fu, Q., Duan, Y., and Wang, G.: Gas-to-Aerosol Phase Partitioning of Atmospheric Water-Soluble Organic Compounds at a Rural Site in China: An Enhancing Effect of NH<sub>3</sub> on SOA Formation, *Environ. Sci. Technol.*, 56, 3915-3924, [10.1021/acs.est.1c06855](https://doi.org/10.1021/acs.est.1c06855), 2022.

710 Meng, J., Liu, X., Hou, Z., Yi, Y., Yan, L., Li, Z., Cao, J., Li, J., and Wang, G.: Molecular characteristics and stable carbon isotope compositions of dicarboxylic acids and related compounds in the urban atmosphere of the North China Plain: Implications for aqueous phase formation of SOA during the haze periods, *Sci. Total Environ.*, 705, 135256, <https://doi.org/10.1016/j.scitotenv.2019.135256>, 2020.

Meng, J., Li, Z., Zhou, R., Chen, M., Li, Y., Yi, Y., Ding, Z., Li, H., Yan, L., Hou, Z., and Wang, G.: Enhanced photochemical formation of secondary organic aerosols during the COVID-19 lockdown in Northern China, *Sci. Total Environ.*, 758, 143709, <https://doi.org/10.1016/j.scitotenv.2020.143709>, 2021.

715 Meng, J., Wang, G., Hou, Z., Liu, X., Wei, B., Wu, C., Cao, C., Wang, J., Li, J., Cao, J., Zhang, E., Dong, J., Liu, J., Ge, S., and Xie, Y.: Molecular distribution and stable carbon isotopic compositions of dicarboxylic acids and related SOA from biogenic sources in the summertime atmosphere of Mt. Tai in the North China Plain, *Atmos. Chem. Phys.*, 18, 15069-15086, [10.5194/acp-18-15069-2018](https://doi.org/10.5194/acp-18-15069-2018), 2018.

720 Meng, J., Wang, G., Li, J., Cheng, C., Ren, Y., Huang, Y., Cheng, Y., Cao, J., and Zhang, T.: Seasonal characteristics of oxalic acid and related SOA in the free troposphere of Mt. Hua, central China: Implications for sources and formation mechanisms, *Science of The Total Environment*, 493, 1088-1097, <http://dx.doi.org/10.1016/j.scitotenv.2014.04.086>, 2014.

Miyazaki, Y., Aggarwal, S. G., Singh, K., Gupta, P. K., and Kawamura, K.: Dicarboxylic acids and water-soluble organic carbon in aerosols in New Delhi, India, in winter: Characteristics and formation processes, *J. Geophys. Res. Atmos.*, 114, D19206, [10.1029/2009jd011790](https://doi.org/10.1029/2009jd011790), 2009.

725 Mochizuki, T., Kawamura, K., Miyazaki, Y., Wada, R., Takahashi, Y., Saigusa, N., and Tani, A.: Secondary formation of oxalic acid and related organic species from biogenic sources in a larch forest at the northern slope of Mt. Fuji, *Atmos. Environ.*, 166, 255-262, <https://doi.org/10.1016/j.atmosenv.2017.07.028>, 2017.

730 Myriokefalitakis, S., Tsigaridis, K., Mihalopoulos, N., Sciare, J., Nenes, A., Kawamura, K., Segers, A., and Kanakidou, M.: In-cloud oxalate formation in the global troposphere: a 3-D modeling study, *Atmos. Chem. Phys.*, 11, 5761-5782, [10.5194/acp-11-5761-2011](https://doi.org/10.5194/acp-11-5761-2011), 2011.

Narukawa, M., Kawamura, K., Takeuchi, N., and Nakajima, T.: Distribution of dicarboxylic acids and carbon isotopic compositions in aerosols from 1997 Indonesian forest fires, *Geophys. Res. Lett.*, 26, 3101-3104, <https://doi.org/10.1029/1999GL010810>, 1999.

735 Pavuluri, C. M. and Kawamura, K.: Evidence for 13-carbon enrichment in oxalic acid via iron catalyzed photolysis in aqueous phase, *Geophysical Research Letters*, 39, L03802, [10.1029/2011gl050398](https://doi.org/10.1029/2011gl050398), 2012.

Pavuluri, C. M. and Kawamura, K.: Enrichment of <sup>13</sup>C in diacids and related compounds during photochemical processing of aqueous aerosols: New proxy for organic aerosols aging, *Sci. Rep.*, 6, 36467, [10.1038/srep36467](https://doi.org/10.1038/srep36467), 2016.

740 Pavuluri, C. M., Kawamura, K., Tachibana, E., and Swaminathan, T.: Elevated nitrogen isotope ratios of tropical Indian aerosols from Chennai: Implication for the origins of aerosol nitrogen in South and Southeast Asia, *Atmospheric Environment*, 44, 3597-3604, <https://doi.org/10.1016/j.atmosenv.2010.05.039>, 2010.

Perri, M. J., Seitzinger, S., and Turpin, B. J.: Secondary organic aerosol production from aqueous photooxidation of glycolaldehyde: Laboratory experiments, *Atmospheric Environment*, 43, 1487-1497, <https://doi.org/10.1016/j.atmosenv.2008.11.037>, 2009.

- Rinaldi, M., Decesari, S., Carbone, C., Finessi, E., Fuzzi, S., Ceburnis, D., O'Dowd, C. D., Sciare, J., Burrows, J. P.,  
745 Vrekoussis, M., Ervens, B., Tsigaridis, K., and Facchini, M. C.: Evidence of a natural marine source of oxalic acid  
and a possible link to glyoxal, *J. Geophys. Res. Atmos.*, 116, n/a-n/a, 10.1029/2011jd015659, 2011.
- Shen, M., Ho, K. F., Dai, W., Liu, S., Zhang, T., Wang, Q., Meng, J., Chow, J. C., Watson, J. G., Cao, J., and Li, J.:  
Distribution and stable carbon isotopic composition of dicarboxylic acids, ketocarboxylic acids and  $\alpha$ -dicarbonyls  
in fresh and aged biomass burning aerosols, *Atmos. Chem. Phys.*, 22, 7489-7504, 10.5194/acp-22-7489-2022,  
750 2022.
- Shi, Z., Song, C., Liu, B., Lu, G., Xu, J., Van Vu, T., Elliott Robert, J. R., Li, W., Bloss William, J., and Harrison Roy, M.:  
Abrupt but smaller than expected changes in surface air quality attributable to COVID-19 lockdowns, *Sci. Adv.*, 7,  
eabd6696, 10.1126/sciadv.abd6696, 2021.
- Sorathia, F., Rajput, P., and Gupta, T.: Dicarboxylic acids and levoglucosan in aerosols from Indo-Gangetic Plain: Inferences  
755 from day night variability during wintertime, *Sci. Total Environ.*, 624, 451-460,  
<https://doi.org/10.1016/j.scitotenv.2017.12.124>, 2018.
- Surratt, J. D., Lewandowski, M., Offenberg, J. H., Jaoui, M., Kleindienst, T. E., Edney, E. O., and Seinfeld, J. H.: Effect of  
Acidity on Secondary Organic Aerosol Formation from Isoprene, *Environ. Sci. Technol.*, 41, 5363-5369,  
10.1021/es0704176, 2007.
- 760 Sun, Y., Wang, Z., Fu, P., Yang, T., Jiang, Q., Dong, H., Li, J., and Jia, J.: Aerosol composition, sources and processes  
during wintertime in Beijing, China, *Atmos. Chem. Phys.*, 13, 4577-4592, 10.5194/acp-13-4577-2013, 2013.
- Wang, G., Cheng, C., Meng, J., Huang, Y., Li, J., and Ren, Y.: Field observation on secondary organic aerosols during Asian  
dust storm periods: Formation mechanism of oxalic acid and related compounds on dust surface, *Atmos. Environ.*,  
113, 169-176, <http://dx.doi.org/10.1016/j.atmosenv.2015.05.013>, 2015.
- 765 Wang, G., Xie, M., Hu, S., Gao, S., Tachibana, E., and Kawamura, K.: Dicarboxylic acids, metals and isotopic compositions  
of C and N in atmospheric aerosols from inland China: implications for dust and coal burning emission and  
secondary aerosol formation, *Atmos. Chem. Phys.*, 10, 6087-6096, 10.5194/acp-10-6087-2010, 2010.
- Wang, G., Kawamura, K., Cheng, C., Li, J., Cao, J., Zhang, R., Zhang, T., Liu, S., and Zhao, Z.: Molecular Distribution and  
Stable Carbon Isotopic Composition of Dicarboxylic Acids, Ketocarboxylic Acids, and  $\alpha$ -Dicarbonyls in  
770 Size-Resolved Atmospheric Particles From Xi 'an City, China, *Environ. Sci. Technol.*, 46, 4783-4791,  
10.1021/es204322c, 2012.
- Wang, G., Zhang, R., Gomez, M. E., Yang, L., Levy Zamora, M., Hu, M., Lin, Y., Peng, J., Guo, S., Meng, J., Li, J., Cheng,  
C., Hu, T., Ren, Y., Wang, Y., Gao, J., Cao, J., An, Z., Zhou, W., Li, G., Wang, J., Tian, P., Marrero-Ortiz, W.,  
Secret, J., Du, Z., Zheng, J., Shang, D., Zeng, L., Shao, M., Wang, W., Huang, Y., Wang, Y., Zhu, Y., Li, Y., Hu, J.,  
775 Pan, B., Cai, L., Cheng, Y., Ji, Y., Zhang, F., Rosenfeld, D., Liss, P. S., Duce, R. A., Kolb, C. E., and Molina, M. J.:  
Persistent sulfate formation from London Fog to Chinese haze, *P. Natl. Acad. Sci. USA*, 113, 13630-13635,  
10.1073/pnas.1616540113, 2016.
- Wang, H. and Kawamura, K.: Stable carbon isotopic composition of low-molecular-weight dicarboxylic acids and ketoacids  
in remote marine aerosols, *J. Geophys. Res. Atmos.*, 111, <https://doi.org/10.1029/2005JD006466>, 2006.
- 780 Wang, H., Huang, C., Tao, W., Gao, Y., Wang, S., Jing, S., Wang, W., Yan, R., Wang, Q., An, J., Tian, J., Hu, Q., Lou, S.,  
Pöschl, U., Cheng, Y., and Su, H.: Seasonality and reduced nitric oxide titration dominated ozone increase during  
COVID-19 lockdown in eastern China, *npj Climate and Atmospheric Science*, 5, 24, 10.1038/s41612-022-00249-3,  
2022.
- Wang, J., Wang, G., Wu, C., Li, J., Cao, C., Li, J., Xie, Y., Ge, S., Chen, J., Zeng, L., Zhu, T., Zhang, R., and Kawamura, K.:  
785 Enhanced aqueous-phase formation of secondary organic aerosols due to the regional biomass burning over North

China Plain, *Environ. Pollut.*, 256, 113401, <https://doi.org/10.1016/j.envpol.2019.113401>, 2020a.

Wang, P., Chen, K., Zhu, S., Wang, P., and Zhang, H.: Severe air pollution events not avoided by reduced anthropogenic activities during COVID-19 outbreak, *Resour. Conserv. Recy.*, 158, 104814, <https://doi.org/10.1016/j.resconrec.2020.104814>, 2020b.

790 Warneck, P.: In-cloud chemistry opens pathway to the formation of oxalic acid in the marine atmosphere, *Atmos. Environ.*, 37, 2423-2427, [http://dx.doi.org/10.1016/S1352-2310\(03\)00136-5](http://dx.doi.org/10.1016/S1352-2310(03)00136-5), 2003.

Weller, C., Tilgner, A., Bräuer, P., and Herrmann, H.: Modeling the Impact of Iron–Carboxylate Photochemistry on Radical Budget and Carboxylate Degradation in Cloud Droplets and Particles, *Environmental Science & Technology*, 48, 5652-5659, 10.1021/es4056643, 2014.

795 Wu, J., Bei, N., Hu, B., Liu, S., Wang, Y., Shen, Z., Li, X., Liu, L., Wang, R., Liu, Z., Cao, J., Tie, X., Molina, L. T., and Li, G.: Aerosol–photolysis interaction reduces particulate matter during wintertime haze events, *P. Natl. Acad. Sci. USA*, 117, 9755-9761, 10.1073/pnas.1916775117, 2020.

Xu, B., Zhang, G., Gustafsson, Ö., Kawamura, K., Li, J., Andersson, A., Bikkina, S., Kunwar, B., Pokhrel, A., Zhong, G., Zhao, S., Li, J., Huang, C., Cheng, Z., Zhu, S., Peng, P., and Sheng, G.: Large contribution of fossil-derived components to aqueous secondary organic aerosols in China, *Nat. Commun.*, 13, 5115, 10.1038/s41467-022-32863-3, 2022.

800 Xu, K., Cui, K., Young, L.-H., Wang, Y.-F., Hsieh, Y.-K., Wan, S., and Zhang, J.: Air Quality Index, Indicator Air Pollutants and Impact of COVID-19 Event on the Air Quality near Central China, *Aerosol and Air Quality Research*, 20, 1204-1221, 10.4209/aaqr.2020.04.0139, 2020.

805 Yu, Q., Chen, J., Cheng, S., Qin, W., Zhang, Y., Sun, Y., and Ahmad, M.: Seasonal variation of dicarboxylic acids in PM<sub>2.5</sub> in Beijing: Implications for the formation and aging processes of secondary organic aerosols, *Sci. Total Environ.*, 763, 142964, <https://doi.org/10.1016/j.scitotenv.2020.142964>, 2021.

Yu, Q., Chen, J., Qin, W., Cheng, S., Zhang, Y., Ahmad, M., and Ouyang, W.: Characteristics and secondary formation of water-soluble organic acids in PM<sub>1</sub>, PM<sub>2.5</sub> and PM<sub>10</sub> in Beijing during haze episodes, *Sci. Total Environ.*, 669, 175-184, <https://doi.org/10.1016/j.scitotenv.2019.03.131>, 2019.

810 Zhang, Y., Kawamura, K., Cao, F., and Lee, M.: Stable carbon isotopic compositions of low-molecular-weight dicarboxylic acids, oxocarboxylic acids,  $\alpha$ -dicarbonyls, and fatty acids: Implications for atmospheric processing of organic aerosols, *J. Geophys. Res. Atmos.*, 121, 3707-3717, 10.1002/2015jd024081, 2016.

Zhang, R., Wang, G., Guo, S., Zamora, M. L., Ying, Q., Lin, Y., Wang, W., Hu, M., and Wang, Y.: Formation of Urban Fine Particulate Matter, *Chemical Reviews*, 115, 3803-3855, 10.1021/acs.chemrev.5b00067, 2015.

815 Zhao, W., Kawamura, K., Yue, S., Wei, L., Ren, H., Yan, Y., Kang, M., Li, L., Ren, L., Lai, S., Li, J., Sun, Y., Wang, Z., and Fu, P.: Molecular distribution and compound-specific stable carbon isotopic composition of dicarboxylic acids, oxocarboxylic acids and  $\alpha$ -dicarbonyls in PM<sub>2.5</sub> from Beijing, China, *Atmos. Chem. Phys.*, 18, 2749-2767, 10.5194/acp-18-2749-2018, 2018.

820 Zhao, W., Ren, H., Kawamura, K., Du, H., Chen, X., Yue, S., Xie, Q., Wei, L., Li, P., Zeng, X., Kong, S., Sun, Y., Wang, Z., and Fu, P.: Vertical distribution of particle-phase dicarboxylic acids, oxoacids and  $\alpha$ -dicarbonyls in the urban boundary layer based on the 325 m tower in Beijing, *Atmos. Chem. Phys.*, 20, 10331-10350, 10.5194/acp-20-10331-2020, 2020.

Zhao, X., Pavuluri, C. M., Dong, Z., Xu, Z., Nirmalkar, J., Jung, J., Fu, P., and Liu, C.-Q.: Molecular Distributions and <sup>13</sup>C Isotopic Composition of Dicarboxylic Acids, Oxocarboxylic Acids, and  $\alpha$ -dicarbonyls in Wintertime PM<sub>2.5</sub> at Three Sites Over Northeast Asia: Implications for Origins and Long-Range Atmospheric Transport, *Journal of Geophysical Research: Atmospheres*, 128, e2023JD038864, <https://doi.org/10.1029/2023JD038864>, 2023.

Zhong, H., Huang, R., Chang, Y., Duan, J., Lin, C., and Chen, Y.: Enhanced formation of secondary organic aerosol from

photochemical oxidation during the COVID-19 lockdown in a background site in Northwest China, *Sci. Total Environ.*, 778, 144947, <https://doi.org/10.1016/j.scitotenv.2021.144947>, 2021.

830

Zhou, Y., Huang, X. H., Bian, Q., Griffith, S. M., Louie, P. K. K., and Yu, J. Z.: Sources and atmospheric processes impacting oxalate at a suburban coastal site in Hong Kong: Insights inferred from 1 year hourly measurements, *Journal of Geophysical Research: Atmospheres*, 120, 9772-9788, <https://doi.org/10.1002/2015JD023531>, 2015.

**Table 1. Meteorological parameters, liquid water content (LWC) of aerosol, in-situ pH (pH<sub>is</sub>), and chemical compositions of PM<sub>2.5</sub> before (January 6 – 23, 2020) and during the lockdown (LCD) (January 31 – February 17, 2020) in Jinan, China.**

	Before the LCD ( <i>n</i> =36)	During the LCD ( <i>n</i> =36)	Whole period ( <i>n</i> =72)
<b>I. Meteorological parameters</b>			
Temperature (°C)	0.07 ± 5.9 (-16–13)	6.8 ± 5.2 (-3.4–16)	3.4 ± 6.5 (-16–16)
Relative humidity (%)	52 ± 10 (30–87)	39 ± 18 (17–85)	45 ± 16 (17–87)
Solar radiation (W m <sup>-2</sup> )	164 ± 70 (32–282)	255 ± 117 (18–423)	209 ± 106 (18–423)
Wind speed (m s <sup>-1</sup> )	3.0 ± 0.7 (1.6–4.6)	3.7 ± 1.1 (1.2–6.6)	3.3 ± 1.0 (1.2–6.6)
<b>II. Gaseous pollutants (µg m<sup>-3</sup>)</b>			
SO <sub>2</sub>	23 ± 8.9 (8.3–49)	14 ± 4.9 (4.9–29)	18 ± 8.5 (4.9–49)
NO <sub>2</sub>	56 ± 12 (38–82)	21 ± 5.9 (9.3–34)	38 ± 20 (9.3–81)
CO	1.6 ± 0.3 (0.9–2.5)	0.9 ± 0.2 (0.5–1.6)	1.3 ± 0.5 (0.5–2.5)
O <sub>3</sub>	29 ± 18 (5.3–74)	66 ± 21 (25–109)	48 ± 27 (5.3–109)
<b>III. Inorganic ions (µg m<sup>-3</sup>)</b>			
K <sup>+</sup>	1.0 ± 0.1 (0.9–1.7)	1.3 ± 0.6 (0.5–2.9)	1.1 ± 0.4 (0.5–2.9)
Na <sup>+</sup>	0.3 ± 0.1 (0.1–0.6)	0.2 ± 0.1 (0.1–0.8)	0.2 ± 0.1 (0.1–0.8)
Ca <sup>2+</sup>	0.4 ± 0.2 (0.1–0.9)	0.5 ± 0.2 (0.2–1.1)	0.5 ± 0.2 (0.1–1.1)
Mg <sup>2+</sup>	0.1 ± 0.03 (0–0.1)	0.1 ± 0.1 (0.1–0.4)	0.1 ± 0.1 (0–0.4)
NH <sub>4</sub> <sup>+</sup>	11 ± 5.7 (4.4–26)	7.7 ± 4.7 (0.4–16)	9.6 ± 5.5 (0.4–26)
NO <sub>3</sub> <sup>-</sup>	19 ± 11 (5.4–49)	9.6 ± 4.9 (1.2–18)	14 ± 9.7 (1.2–49)
SO <sub>4</sub> <sup>2-</sup>	13 ± 6.9 (3.8–31)	9.4 ± 5.3 (1.1–18)	11 ± 6.4 (1.1–31)
SNA <sup>a</sup>	44 ± 23 (15–105)	27 ± 15 (2.8–50)	35 ± 21 (2.8–105)
Subtotal	49 ± 24 (18–113)	35 ± 18 (6.1–67)	42 ± 22 (6.1–113)
<b>IV. Carbonaceous species (µg m<sup>-3</sup>)</b>			
EC	4.3 ± 2.4 (0.9–11)	1.9 ± 1.0 (0.3–3.8)	3.1 ± 2.2 (0.3–11)
OC	10 ± 3.0 (5.2–19)	6.4 ± 2.6 (2.0–11)	8.3 ± 3.4 (2.0–19)
WSOC	3.9 ± 1.9 (1.2–10)	3.2 ± 1.4 (1.0–7.0)	3.5 ± 1.7 (1.0–10)
OC/EC	2.9 ± 1.3 (1.5–6.9)	4.0 ± 1.5 (2.4–8.4)	3.5 ± 1.5 (1.5–8.4)
WSOC/OC	0.4 ± 0.1 (0.2–0.7)	0.5 ± 0.1 (0.3–0.8)	0.4 ± 0.1 (0.2–0.8)
<b>V. Other species</b>			
PM <sub>2.5</sub> (µg m <sup>-3</sup> )	106 ± 45 (35–202)	56 ± 29 (10–111)	81 ± 46 (10–202)
PM <sub>10</sub> (µg m <sup>-3</sup> )	147 ± 58 (38–285)	72 ± 33 (19–129)	109 ± 60 (19–285)
Levogluconan (ng m <sup>-3</sup> )	141 ± 70 (50–370)	102 ± 29 (61–186)	121 ± 57 (50–370)
pH <sub>is</sub>	3.2 ± 3.0 (2.3–7.7)	3.5 ± 3.5 (2.8–4.9)	3.3 ± 3.1 (2.3–7.7)
LWC (µg m <sup>-3</sup> )	35 ± 33 (4.3–172)	10 ± 10 (0.2–45)	24 ± 30 (0.2–172)
SNA/PM <sub>2.5</sub> (%)	40 ± 6.5 (29–54)	47 ± 8.2 (28–60)	43 ± 8.1 (28–60)
N/S <sup>b</sup>	1.5 ± 0.3 (0.9–2.4)	1.1 ± 0.2 (0.7–1.5)	1.3 ± 0.4 (0.7–2.4)

<sup>a</sup>Total concentration of SO<sub>4</sub><sup>2-</sup>, NO<sub>3</sub><sup>-</sup>, and NH<sub>4</sub><sup>+</sup>.<sup>b</sup>The ratio of NO<sub>3</sub><sup>-</sup>/SO<sub>4</sub><sup>2-</sup>.

**Table 2. Concentrations (ng m<sup>-3</sup>) of dicarboxylic acids, oxocarboxylic acids, and  $\alpha$ -dicarbonyls in PM<sub>2.5</sub> before and during the LCD in Jinan.**

Compounds	Before the LCD ( <i>n</i> = 36)	During the LCD ( <i>n</i> = 36)	Whole period ( <i>n</i> = 72)
<b>I. Dicarboxylic acids</b>			
Oxalic, C <sub>2</sub>	181 ± 48 (110–381)	239 ± 108 (46–478)	210 ± 88 (46–478)
Malonic, C <sub>3</sub>	15 ± 4.3 (5.2–26)	45 ± 14 (18–79)	30 ± 19 (5.2–79)
Succinic, C <sub>4</sub>	54 ± 29 (15–178)	30 ± 13 (11–66)	42 ± 25 (11–178)
Glutaric, C <sub>5</sub>	6.7 ± 4.5 (0.6–20)	7.5 ± 4.0 (0.7–15)	7.1 ± 4.2 (0.6–20)
Adipic, C <sub>6</sub>	9.2 ± 8.6 (1.7–41)	6.1 ± 3.3 (0.9–14)	7.6 ± 6.7 (0.9–41)
Pimelic, C <sub>7</sub>	2.3 ± 1.5 (0.2–7.4)	1.9 ± 1.4 (0–5.1)	2.1 ± 1.5 (0–7.4)
Suberic, C <sub>8</sub>	7.7 ± 4.7 (1.9–23)	3.0 ± 2.4 (0.1–13)	5.4 ± 4.4 (0.1–23)
Azelaic, C <sub>9</sub>	12 ± 4.0 (5.8–24)	5.9 ± 4.8 (0.4–23)	9.0 ± 5.3 (0.4–24)
Sebacic, C <sub>10</sub>	3.9 ± 2.3 (1.3–9.9)	2.6 ± 1.5 (0.2– 5.1)	3.3 ± 2.0 (0.2– 9.9)
Undecanedioic, C <sub>11</sub>	4.0 ± 2.9 (0.5–15)	3.5 ± 1.9 (0.3–8.6)	3.8 ± 2.4 (0.3–15)
Methylmalonic, iC <sub>4</sub>	3.5 ± 4.1 (0.2–13)	4.8 ± 4.6 (0–17)	4.1 ± 4.4 (0–17)
Methylsuccinic, iC <sub>5</sub>	4.2 ± 3.5 (0.4–12)	3.4 ± 1.6 (0.4–6.1)	3.8 ± 2.7 (0.4–12)
Methylglutaric, iC <sub>6</sub>	2.2 ± 1.1 (0.4–5.6)	2.4 ± 1.4 (0–6.6)	2.3 ± 1.3 (0–6.6)
Maleic, M	6.9 ± 6.2 (0.8–34)	5.0 ± 2.3 (0.6–11.0)	5.9 ± 4.7 (0.6–34)
Fumaric, F	10 ± 7.6 (2.3–44)	1.5 ± 0.9 (0.2–4.8)	5.8 ± 6.9 (0.2–44)
Methylmaleic, mM	5.5 ± 4.3 (1.4–22)	4.2 ± 3.3 (0–16)	4.9 ± 3.9 (0–22)
Phthalic, Ph	11 ± 6.1 (2.9–34)	8.8 ± 6.1 (1.2–25)	9.9 ± 6.2 (1.2–34)
Isophthalic, iPh	3.0 ± 3.9 (0.2–24)	1.8 ± 2.4 (0–9.9)	2.4 ± 3.3 (0–24)
Terephthalic, tPh	2.0 ± 1.4 (0.2–7.5)	1.3 ± 0.8 (0.1–2.6)	1.6 ± 1.2 (0.1–7.5)
Ketomalonic, kC <sub>3</sub>	2.1 ± 1.4 (0.3–6.3)	3.0 ± 1.7 (0.2–7.4)	2.6 ± 1.6 (0.2–7.4)
Ketopimelic, kC <sub>7</sub>	5.1 ± 4.7 (0.8–20)	5.7 ± 4.2 (0.2–17)	5.4 ± 4.4 (0.2–20)
Subtotal	351 ± 92 (212–672)	386 ± 127 (121–707)	369 ± 112 (121–707)
<b>II. Oxocarboxylic acids</b>			
Pyruvic, Pyr	13 ± 4.9 (4.4–25)	21 ± 8.8 (7.3–43)	17 ± 8.2 (4.4–43)
Glyoxylic, ωC <sub>2</sub>	24 ± 9.1 (6.6–43)	29 ± 8.5 (10–43)	26 ± 9.0 (6.6–43)
3-Oxopropanoic, ωC <sub>3</sub>	4.5 ± 4.6 (0.8–25)	12 ± 6.5 (0.6–27)	8.4 ± 6.9 (0.6–27)
4-Oxobutanoic, ωC <sub>4</sub>	7.1 ± 6.4 (0.8–38)	3.1 ± 2.7 (0–12)	5.1 ± 5.3 (0–38)
7-Oxoheptanoic, ωC <sub>7</sub>	2.3 ± 2.2 (0.2–8.6)	1.9 ± 2.0 (0–8.6)	2.1 ± 2.1 (0–8.6)
8-Oxooctanoic, ωC <sub>8</sub>	3.2 ± 2.8 (0.4–16)	3.7 ± 2.1 (0.1–9.3)	3.4 ± 2.4 (0.1–16)
9-Oxononanoic, ωC <sub>9</sub>	6.9 ± 3.0 (1.5–15)	3.4 ± 2.9 (0–9.0)	5.2 ± 3.4 (0–15)
Subtotal	61 ± 20 (25–106)	75 ± 17 (37–104)	68 ± 19 (25–106)
<b>III. <math>\alpha</math>-Dicarbonyls</b>			
Glyoxal, Gly	13 ± 6.3 (4.4–32)	13 ± 5.3 (2.0–28)	13 ± 5.8 (2.0–32)
Methylglyoxal, mGly	12 ± 7.6 (2.6–30)	12 ± 4.8 (2.4–21)	12 ± 6.0 (2.4–30)
Subtotal	25 ± 14 (7.8–62)	25 ± 10 (4.4–49)	25 ± 12 (4.4–62)
Total detected species	437 ± 117 (246–833)	486 ± 144 (179–825)	461 ± 132 (179–833)

**Table 3. Differences in the stable carbon isotopic compositions ( $\delta^{13}\text{C}$ , ‰) of major detected diacids and related compounds before and during the LCD.**

Compounds	Before the LCD ( $n = 36$ )	During the LCD ( $n = 36$ )	Whole period ( $n = 72$ )
<b>I. Dicarboxylic acids</b>			
C <sub>2</sub>	$-22 \pm 1.9$ (-26 to -17)	$-19 \pm 2.5$ (-24 to -14)	$-20 \pm 2.5$ (-26 to -14)
C <sub>3</sub>	$-25 \pm 4.2$ (-36 to -19)	$-23 \pm 2.2$ (-26 to -18)	$-24 \pm 3.6$ (-36 to -18)
C <sub>4</sub>	$-28 \pm 4.6$ (-39 to -22)	$-25 \pm 2.4$ (-29 to -20)	$-26 \pm 4.0$ (-39 to -20)
C <sub>6</sub>	$-29 \pm 3.4$ (-38 to -23)	$-27 \pm 2.8$ (-31 to -22)	$-28 \pm 3.3$ (-38 to -22)
C <sub>9</sub>	$-27 \pm 1.2$ (-30 to -25)	$-27 \pm 2.3$ (-32 to -24)	$-27 \pm 1.8$ (-32 to -24)
Ph	$-39 \pm 6.4$ (-51 to -27)	$-30 \pm 2.6$ (-36 to -26)	$-34 \pm 6.4$ (-51 to -26)
tPh	$-37 \pm 4.1$ (-46 to -26)	$-34 \pm 0.9$ (-36 to -32)	$-35 \pm 3.1$ (-46 to -26)
<b>II. Oxocarboxylic acids</b>			
Pyr	$-28 \pm 4.0$ (-39 to -22)	$-24 \pm 2.3$ (-29 to -20)	$-26 \pm 3.9$ (-39 to -20)
$\omega\text{C}_2$	$-27 \pm 3.6$ (-38 to -22)	$-23 \pm 2.2$ (-26 to -19)	$-25 \pm 3.6$ (-38 to -19)
$\omega\text{C}_3$	$-29 \pm 4.0$ (-40 to -24)	$-26 \pm 2.3$ (-30 to -22)	$-28 \pm 3.7$ (-40 to -22)
<b>III. <math>\alpha</math>-Dicarbonyls</b>			
Gly	$-23 \pm 3.7$ (-36 to -19)	$-20 \pm 2.2$ (-24 to -16)	$-21 \pm 3.5$ (-36 to -16)
mGly	$-25 \pm 3.8$ (-37 to -21)	$-21 \pm 2.0$ (-25 to -18)	$-23 \pm 3.6$ (-37 to -18)



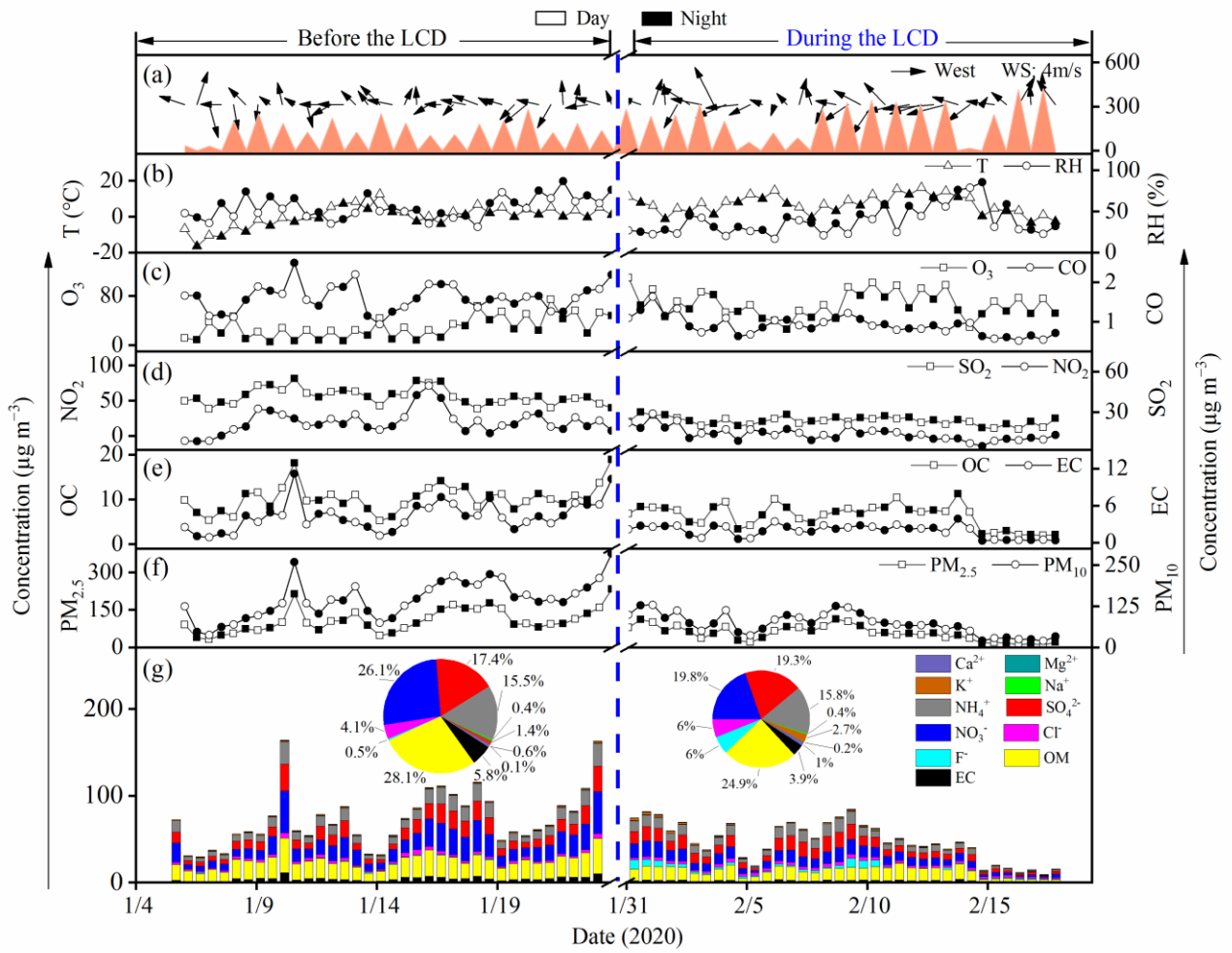


Figure 1. Temporal variations of gaseous pollutants, meteorological parameters, and chemical compositions of PM<sub>2.5</sub> before and during the LCD.

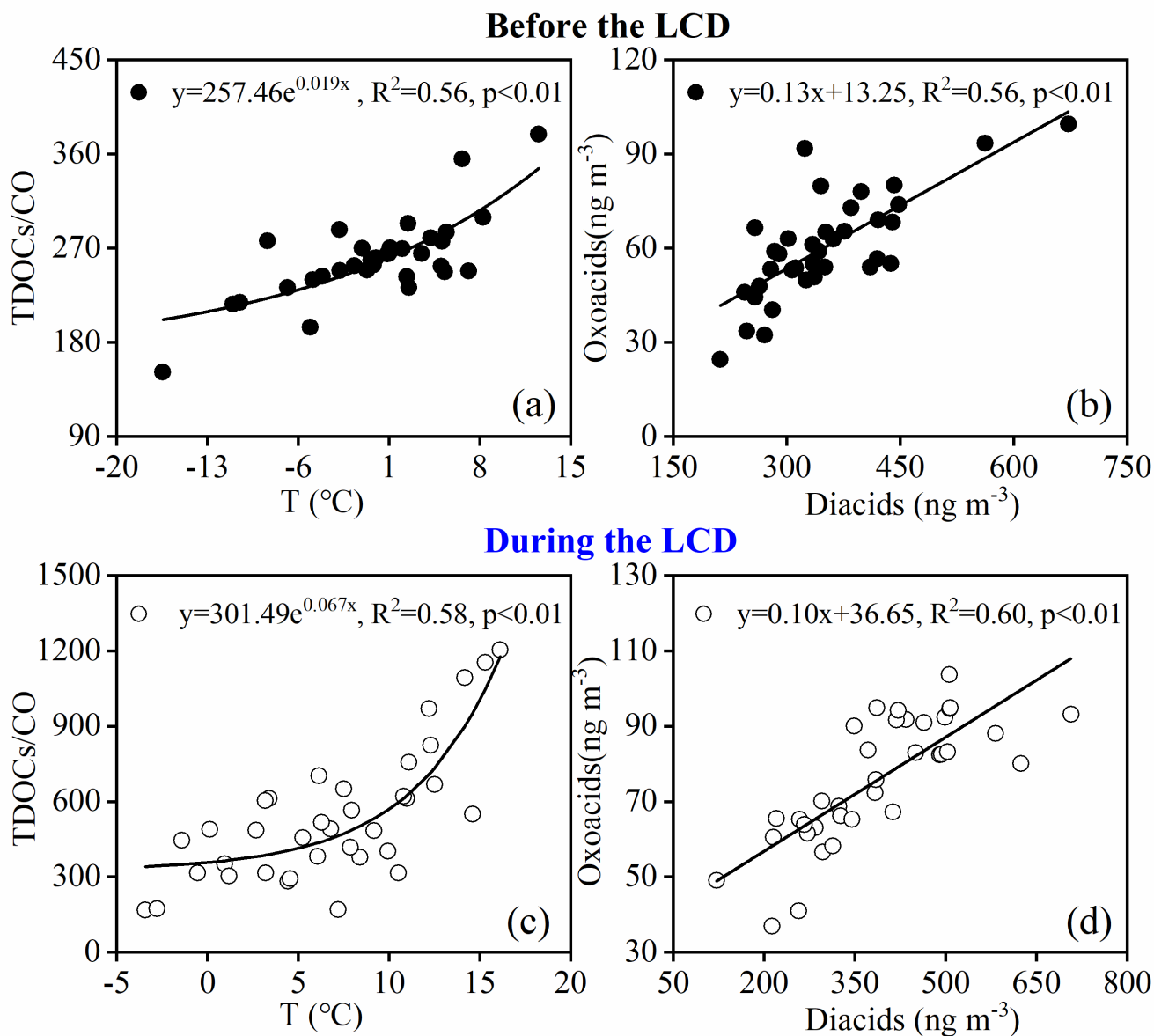


Figure 2. Correlation analysis between the ratio of total concentration of detected organic components (TDOCs) normalized by CO (TDOCs/CO) and temperature, and between diacids and oxoacids (a) and (b) before the LCD, (c) and (d) during the LCD.

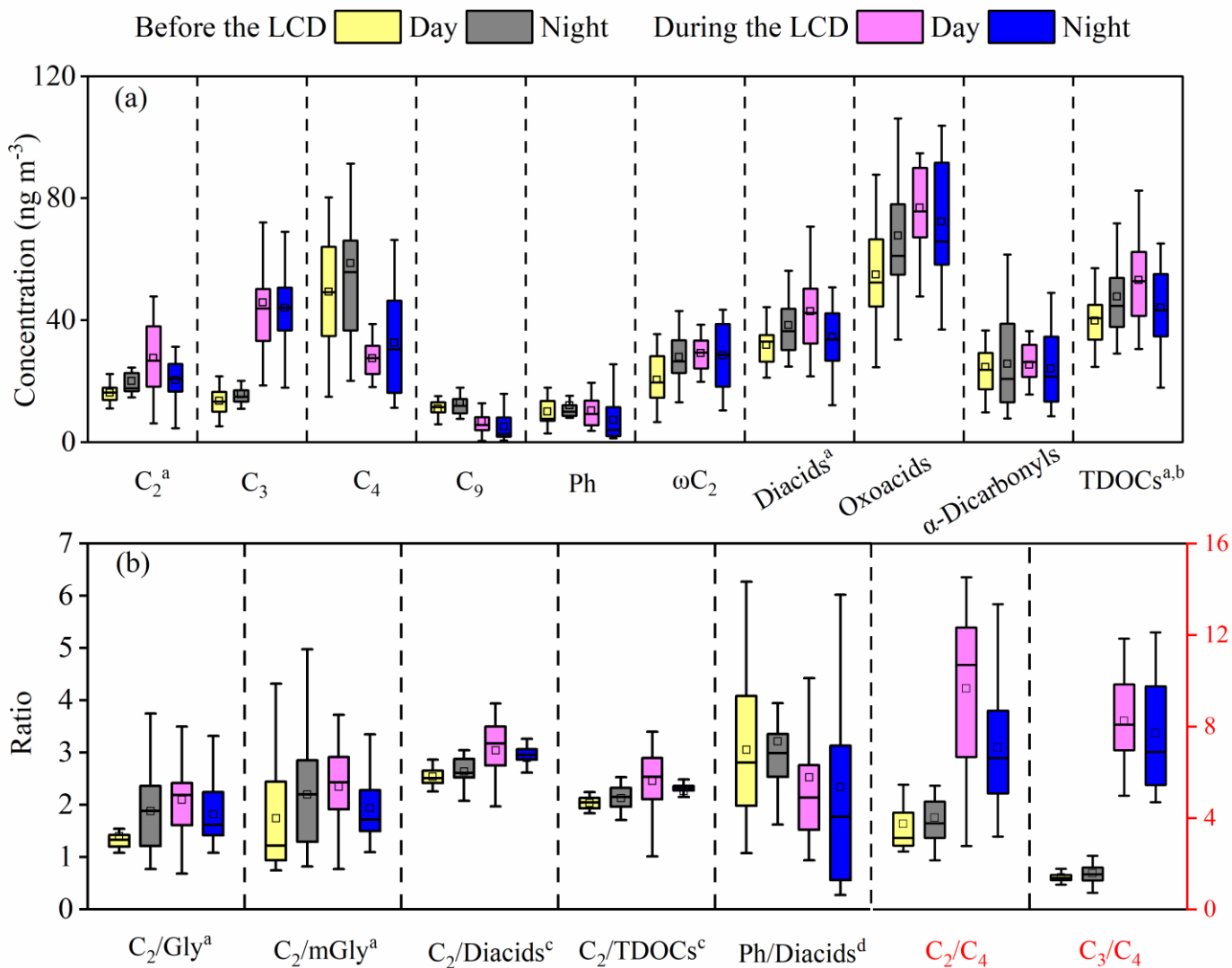
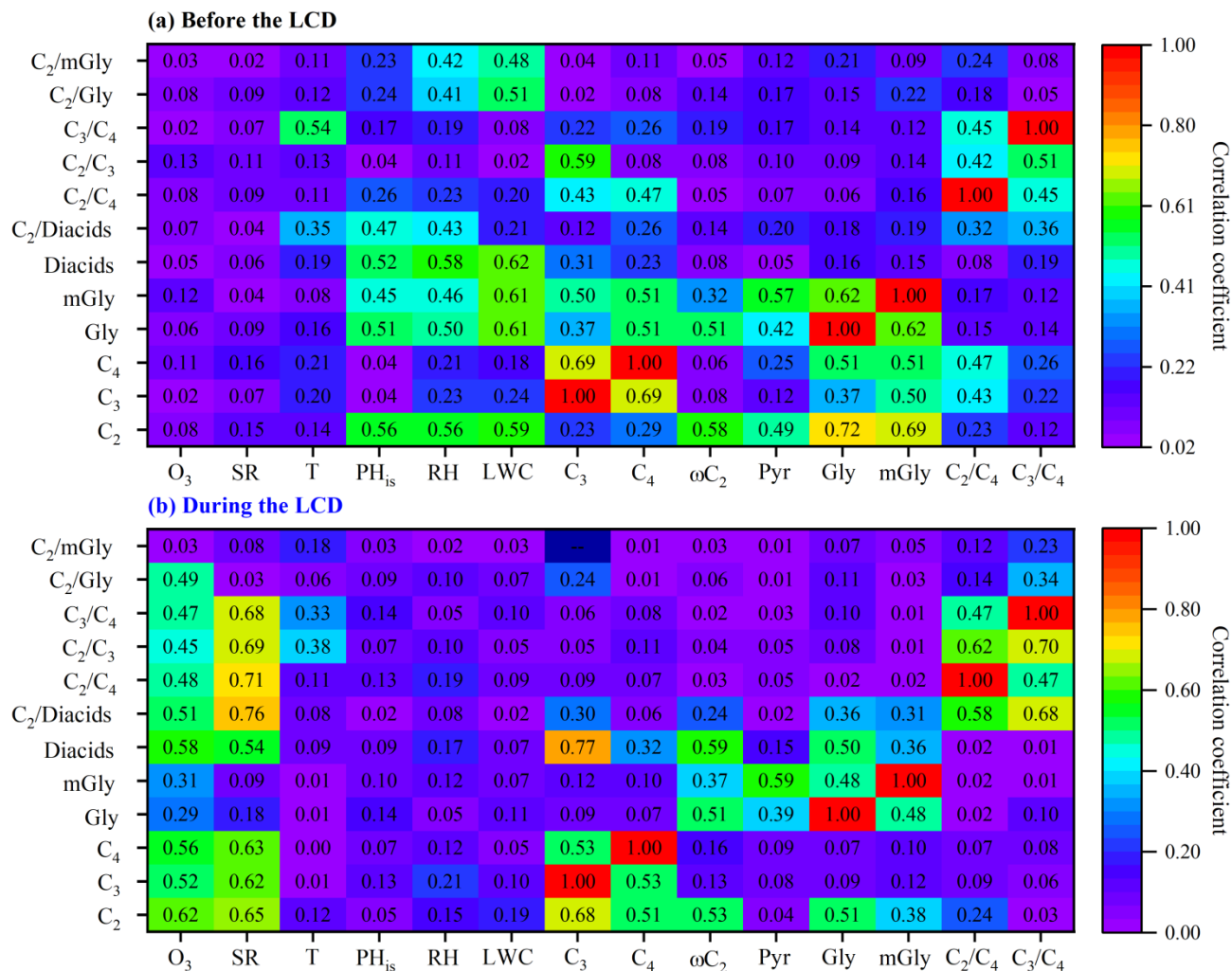
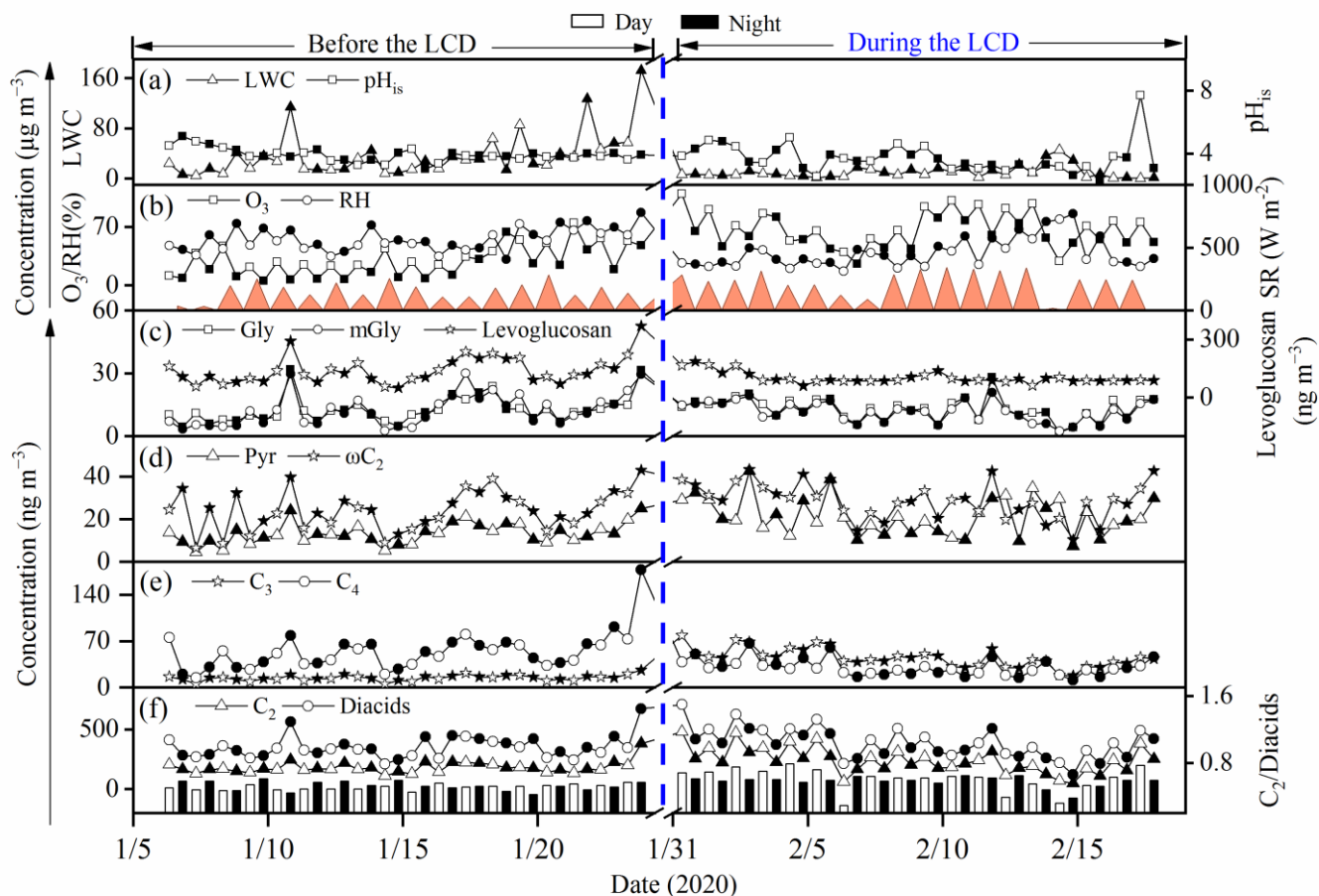


Figure 3. Diurnal changes of (a) major organic compounds and (b) selected mass ratios before and during the LCD (<sup>a</sup> the concentrations reduced by 10 times; <sup>b</sup> TDOCs: total detected organic components; <sup>c</sup> the mass ratios enlarged by 5 times; <sup>d</sup> the mass ratio enlarged by 100 times).



**Figure 4.** Correlation coefficients ( $R^2$ ) of concentrations of C<sub>2</sub> and its organic precursors and selected ratios with influencing factors (a) before the LCD and (b) during the LCD.



**Figure 5.** Temporal variations in the concentrations of levoglucosan, diacids,  $C_2$  and its major precursors, the ratios of  $C_2$ /Diacids, as well as liquid water content (LWC), in-situ pH ( $pH_{is}$ ), temperature, relative humidity (RH), solar radiation, and  $O_3$  before and during the LCD.

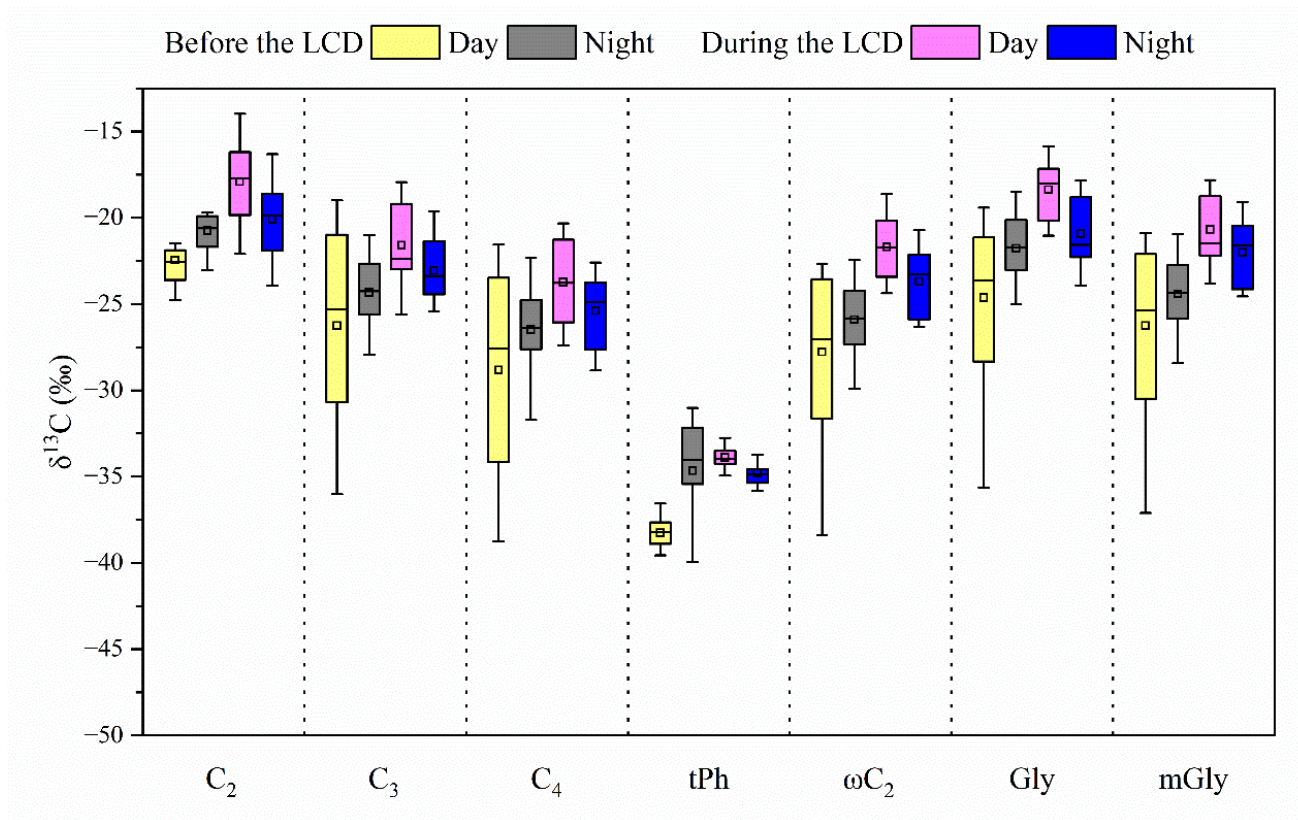
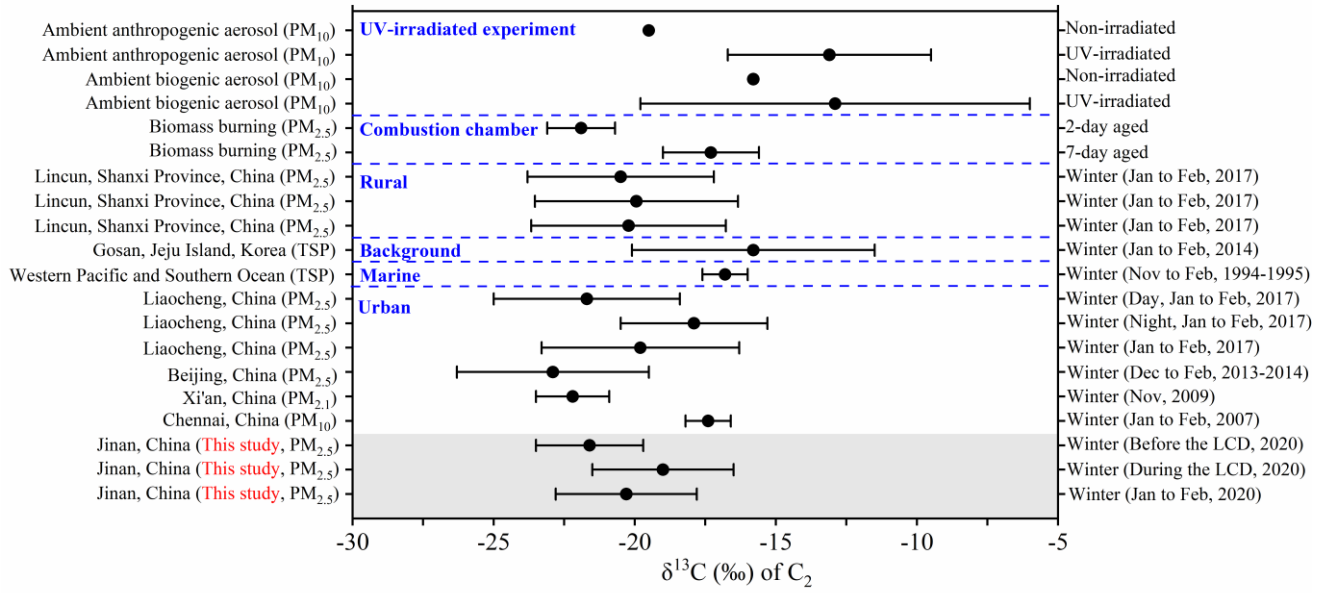
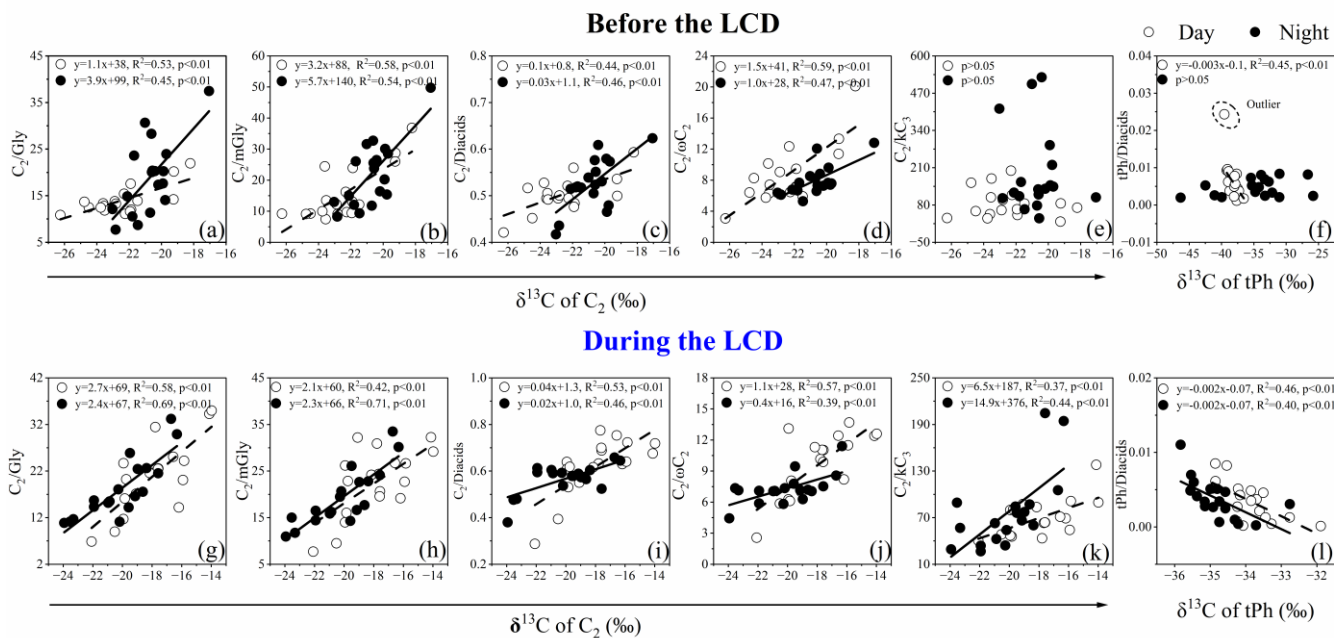


**Figure 6.** Differences in the stable carbon isotope compositions of major detected diacids ( $\text{C}_2$ – $\text{C}_4$ , tPh), the smallest oxoacids ( $\omega\text{C}_2$ ), and  $\alpha$ -dicarbonyls including Gly and mGly before and during the LCD in the atmosphere of Jinan.



875

**Figure 7. Comparison of stable carbon isotopic compositions ( $\delta^{13}\text{C}$ , ‰) of  $\text{C}_2$  in aerosols of Jinan with those in other regions in the winter.**



880 **Figure 8.** Correlations of the  $\delta^{13}\text{C}$  of  $\text{C}_2$  with the mass ratios of  $\text{C}_2/\text{Gly}$ ,  $\text{C}_2/\text{mGly}$ ,  $\text{C}_2/\text{Diacids}$ ,  $\text{C}_2/\omega\text{C}_2$ , and  $\text{C}_2/\text{kC}_3$ , and the  $\delta^{13}\text{C}$  of tPh with the mass ratio of tPh/Diacids before and during the LCD in January to February 2020.



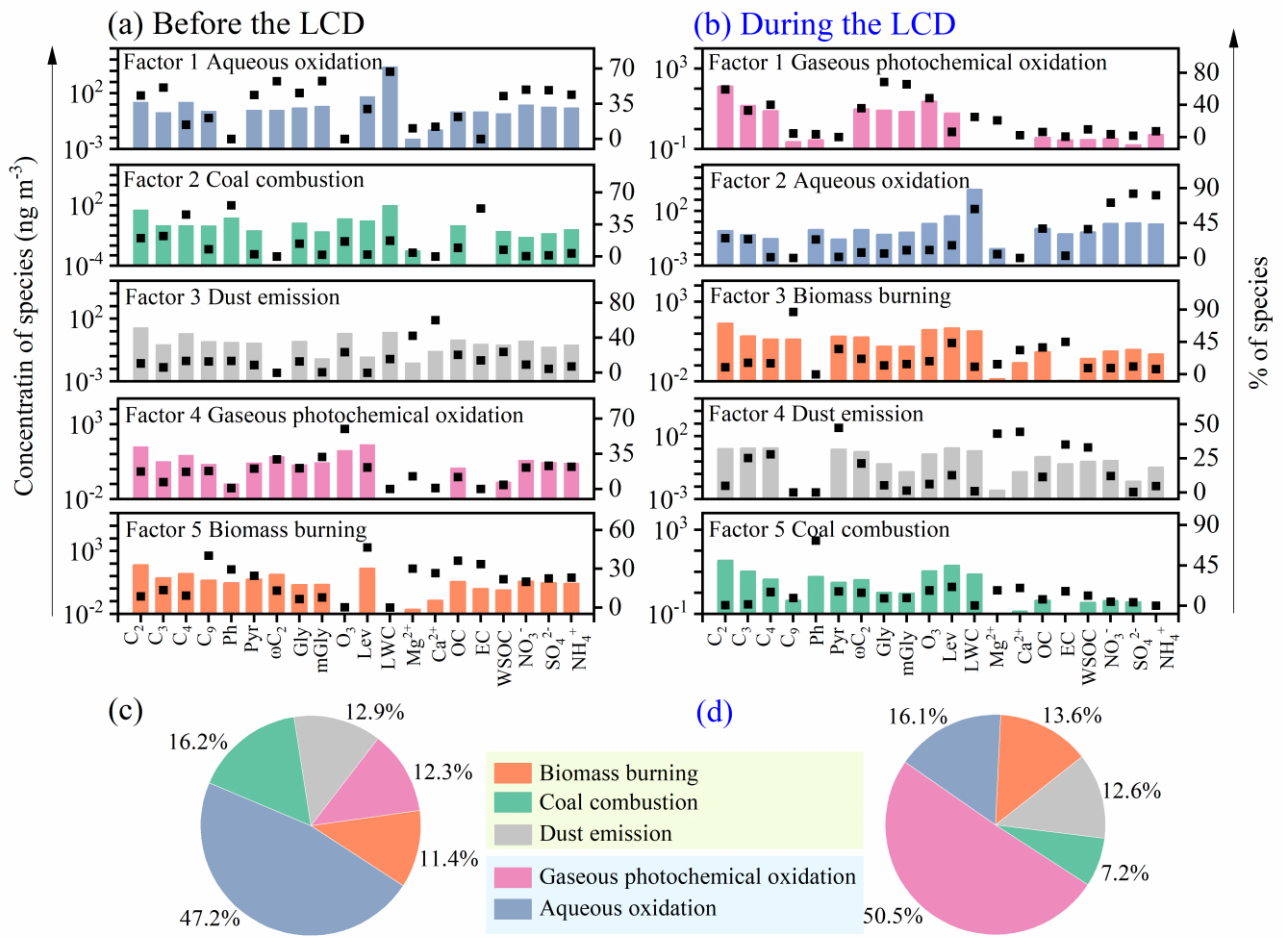


Figure 9. Source profiles of major chemical components in the  $\text{PM}_{2.5}$  samples from Jinan (a, c) before the LCD and (b, d) during the LCD (BB: biomass burning).

885